Human Molecular Genetics, 2021, Vol. 30, No. 17 1632–1648

https://doi.org/10.1093/hmg/ddab143
Advance Access Publication Date: 2 June 2021
General Article

GENERAL ARTICLE

Small molecule *1a* reduces FMRpolyG-mediated toxicity in *in vitro* and *in vivo* models for *FMR1* premutation

Saif N. Haify[1,†,*], Ronald A.M. Buijsen[1,2,†], Lucas Verwegen[1,3,†], Lies-Anne W.F.M. Severijnen[1], Helen de Boer[1], Valerie Boumeester[1], Roos Monshouwer[1], Wang-Yong Yang[4], Michael D. Cameron[4], Rob Willemsen[1], Matthew D. Disney[4] and Renate K. Hukema[1,5]

[1]Department of Clinical Genetics, Erasmus MC, Rotterdam 3015 GD, The Netherlands, [2]Department of Human Genetics, LUMC, Leiden 2300 RC, The Netherlands, [3]Department of Cell Biology, Erasmus MC, Rotterdam 3015 GD, The Netherlands, [4]Department of Chemistry, Scripps Research Institute, FL 33458, USA and [5]Department of Health Care Studies, Rotterdam University of Applied Sciences, Rotterdam 3015 GG, The Netherlands

*To whom correspondence should be addressed. Email: s.haify@erasmusmc.nl

Abstract

Fragile X-associated tremor and ataxia syndrome (FXTAS) is a late-onset, progressive neurodegenerative disorder characterized by tremors, ataxia and neuropsychological problems. This disease is quite common in the general population with approximately 20 million carriers worldwide. The risk of developing FXTAS increases dramatically with age, with about 45% of male carriers over the age of 50 being affected. FXTAS is caused by a CGG-repeat expansion (CGG_{exp}) in the fragile X mental retardation 1 (*FMR1*) gene. CGG_{exp} RNA is translated into the FMRpolyG protein by a mechanism called RAN translation. Although both gene and pathogenic trigger are known, no therapeutic interventions are available at this moment. Here, we present, for the first time, primary hippocampal neurons derived from the ubiquitous inducible mouse model which is used as a screening tool for targeted interventions. A promising candidate is the repeat binding, RAN translation blocking, small molecule *1a*. Small molecule *1a* shields the disease-causing CGG_{exp} from being translated into the toxic FMRpolyG protein. Primary hippocampal neurons formed FMRpolyG-positive inclusions, and upon treatment with *1a*, the numbers of FMRpolyG-positive inclusions are reduced. We also describe for the first time the formation of FMRpolyG-positive inclusions in the liver of this mouse model. Treatment with *1a* reduced the insoluble FMRpolyG protein fraction in the liver but not the number of inclusions. Moreover, *1a* treatment had a reducing effect on the number of Rad23b-positive inclusions and insoluble Rad23b protein levels. These data suggest that targeted small molecule therapy is effective in an FXTAS mouse model and has the potential to treat CGG_{exp}-mediated diseases, including FXTAS.

[†]These authors contributed equally to this work.

Received: September 10, 2020. **Revised:** May 13, 2021. **Accepted:** May 15, 2021

Introduction

Fragile X-associated tremor and ataxia syndrome (FXTAS) is a late-onset neurodegenerative disorder. FXTAS was first described in 2001 and is clinically characterized by progressive intention tremors and cerebellar gait ataxia. More severe cases include progressive cognitive decline, Parkinsonism, autonomic dysfunction and a spectrum of neuropsychiatric disorders (1–4). FXTAS neuropathology includes mild brain atrophy, loss of Purkinje neurons and Bergmann gliosis (4–6). Life expectancy is estimated to be between 5 and 25 years after the disease onset (7). In the post-mortem brain tissue from patients with FXTAS, the major pathological hallmark is the presence of ubiquitin-positive intranuclear inclusions throughout the brain, in both neurons and astrocytes (7,8). Pathology is not only limited to the central nervous system, but intranuclear inclusions are also found in the non-central nervous system organs (9–15). FXTAS is caused by a trinucleotide expansion of the CGG repeat (CGG_{exp}) in the 5′-untranslated region (UTR) of the fragile X mental retardation 1 (*FMR1*) gene (1,16). Healthy individuals have repeat numbers ranging from 5 to 55 CGGs. The repeat can expand throughout generations owing to its instable nature to lengths varying from 55 to 200 CGGs in number (17). These individuals are often referred to as premutation (PM) carriers. PM carriers have 2- to 8-fold elevated levels of *FMR1* mRNA and paradoxically slightly decreased fragile X mental retardation protein (FMRP) levels (18–20). Approximately, 45% of male PM carriers over the age of 50 will eventually develop FXTAS, while between 8% and 16% of female PM carriers will develop FXTAS and are also at the risk of developing fragile X-associated primary ovarian insufficiency (FXPOI) (21,22). The partial protective influence of the second non-expanded allele in female carriers results in a lower penetrance.

Although the exact mechanism of FXTAS remains unclear, it is generally accepted that two mechanisms most likely contribute to FXTAS pathogenesis (23). A first mechanism is the toxic RNA gain-of-function mechanism that is supported by elevated levels of *FMR1* mRNA bearing a CGG_{exp} that by itself is toxic to cells. In this mechanism, CG-rich expansion transcripts form secondary hairpin-like structures that can sequester RNA-binding proteins (RBPs), such as the Src-associated substrate, in the mitosis of 68 kDa (SAM68), DROSHA and DGCR8 and the heterogeneous nuclear ribonucleoprotein (hnRNP) sequester in inclusions, resulting in the depletion of these proteins in the cell, disturbing critical processes causing aberrant miRNA processing, altered RNA splicing, integrated stress response (ISR) and immune effects (24–27). When analyzing the post-mortem brain tissue of FXTAS patients, *FMR1* mRNA is found in intranuclear inclusions as well as in isolated nuclei (14,24).

The second mechanism is a protein gain-of-function mechanism as a result of repeat-associated non-AUG (RAN) translation, which was first described for FXTAS in 2013 (28–30). The mechanistic understanding of RAN translation and RAN proteins in FXTAS has increased tremendously through the use of cell models and several animal models. RAN translation in FXTAS initiates in a cap-dependent manner at a non-AUG near cognate start-codon (ACG) located before the CGG_{exp} in the 5′-UTR region of the *FMR1* gene (29). Initiation in the +0 frame (FMRpolyR) can occur at an ACG codon located upstream of the repeat insertion site. However, FMRpolyR production is less than 1% of FMRpolyG expression (31). Initiation in the +2 reading frame occurs within the repeat itself and results in a FMRpolyA protein. More recently, evidence was found suggesting that the ISR, which is known to effectively inhibit global canonical translation, also selectively up-regulates RAN translation in repeat expansion diseases (32). Several overexpressing animal models have shown that FMRpolyG can be toxic and can result in FXTAS disease-like phenotypes (29,33). Toxicity of the FMRpolyG protein has also been linked with the impairment of the ubiquitination proteasome degradation system (UPS) (34). Several studies have shown that the FMRpolyG protein together with other prominent proteins, such as HSP40, Rad23b and the 20S subunit of the proteasome, were found within intranuclear inclusions in several FXTAS animal models as well as in patient brain tissue. Intranuclear inclusions containing different toxic polypeptides have been linked with the neuronal degradation in other neurodegenerative diseases (10,29,33,35–39). In fact, for some neurodegenerative diseases, RAD23B is proposed as a neuropathological hallmark like in Huntington's disease (HD), Parkinson's disease (PD) and several spinocerebellar ataxias (SCA), like SCA3 and SCA7 (38).

To understand the contribution of repeat bearing RNA molecules and the FMRpolyG protein in FXTAS, we and others have generated various mouse models (33,35,36,40). Sellier and colleagues generated a mouse model expressing high levels of RNA with and without FMRpolyG expression. Mice with FMRpolyG expression showed locomotor deficits, including decreased mobility and obesity, and died at 10 months of age, suggesting a direct role for FMRpolyG in CGG–RNA repeat-associated toxicity (35). In addition, the RNA-only mice showed no disease phenotype, suggesting that the translation of expanded CGG repeats into FMRpolyG drives the pathogenesis in FXTAS.

Even though we have a fair understanding of the pathological mechanisms underlying FXTAS, there is no current cure available to stop disease progression in FXTAS patients. However, there are symptomatic therapies available for FXTAS patients. Certain medications that are usually associated with other diseases help slow down the progression of several symptoms seen in FXTAS patients (2). For example, FXTAS patients with severe intention tremors could respond well to β-blockers, primidone and topiramate. Moreover, intention tremors are aggravated by anxiety and stress, which are also symptoms often seen in FXTAS patients. Benzodiazepines, such as alprazolam, may therefore in some cases of FXTAS also be effective in treating anxiety and tremors (41). Our proof-of-concept study in an inducible mouse model suggests that an early intervention might be beneficial for FXTAS patients and PM carriers. We can halt disease progression by stopping mutant RNA expression in a brain-specific inducible mouse model. Strikingly, stopping mutant RNA expression early in the disease process results in the reversibility of neuropathology, including the number of intranuclear inclusions (36).

Previously, we reported a small chemical compound, *1a*, targeting the mRNA containing the expanded CGG repeat (CGG_{exp}). Compound *1a* shields the CGG repeat by binding GG-mismatch binding spots, preventing both the binding of RBPs to the hairpin structure and RAN translation. *In vitro*, the compound showed promising results in transfected COS7 cells by improving the FXTAS-associated pre-mRNA splicing defects and by reducing the size and number of protein aggregates in COS7 cells (42).

To test the potential of compound *1a* in more disease-relevant neuronal cellular model, we generated primary hippocampal neuronal cultures originating from an FXTAS mouse model. Here, we show that treatment using compound *1a* partially prevents the inclusion formation in these neuronal cells. Moreover, we showed the rapid formation of inclusions in the liver of FXTAS mice ubiquitously expressing FMRpolyG,

which makes this a useful model for quick testing for intervention methods (42–44). Next, we tested the potential of compound *1a in vivo*. Our data show a clear effect on the FMRpolyG-insoluble protein levels in these mice. These results will contribute to the general understanding of FMRpolyG toxicity and will initiate the first steps in developing a potential new therapy.

Materials and Methods

Mice

Transgenic mice used in this study were obtained by crossing TRE-90 CGG-eGFP mice with hnRNP-rtTA driver mice (40). The TRE-90 CGG-eGFP mice express the enhanced green fluorescent protein (eGFP) under the control of a tetracycline-responsive promoter element (TRE). Before the eGFP sequence, a human *FMR1* 5′UTR containing 90 CGG repeats was placed. Normally, this transgene translates into eGFP, but RAN translation may result in the production of FMRpolyG. Therefore, mRNA of this transgene translates into either eGFP (canonical translation) or FMRpolyG (RAN translation), much like *FMR1* mRNA in FXTAS can translate into either FMRP or FMRpolyG. Over multiple generations, we never observed any repeat instability in these mice. The hnRNP-rtTA driver mice express the reverse tetracycline transcriptional activator (rtTA) under the control of a ubiquitously expressed hnRNP promoter, able to activate the TRE in the presence of dox. Both transgenic mouse lines were generated in a C57BL/6JRj background. Heterozygous mice from both lines were crossed to obtain double transgenic TRE-90 CGG-eGFP/hnRNP-rtTA mice (hereafter, referred to as DT mice) as well as non-transgenic or single transgenic littermate controls (hereafter, referred to as NT mice). Animals were treated with dox [2 mg/ml doxycycline hyclate (Sigma) and 5% sucrose (Sigma)] or only sucrose (5% sucrose) in their drinking water, starting between the ages of P24 and 27. Drinking water was kept from light and refreshed every 2–3 days to guarantee the stability of dox. Mice treated with the compound *1a* (6.6 mg/ml in DMSO) were given a single intra-peritoneal (IP) injection at a dose of 10 mg/kg simultaneous with dox induction. Animals injected with vehicle (DMSO) were used as control for compound *1a*. Owing to the toxic nature of DMSO, its concentration was kept low. Animals in the experiment were sacrificed upon sudden weight loss, or 7 days after dox induction. Mice were housed at the Erasmus MC animal facility (Rotterdam, The Netherlands), under standard housing and husbandry conditions. All experiments were approved by the local welfare committee under license number AVD10100201529 and protocol number 15-290-05.

Genotyping

For regular genotyping, toe clips from the P5-7 mice were incubated overnight in 300 µl of tail digestion buffer [TDB; 50 mM KCl, 10 mM of Tris–HCl, pH 9, 0.1% Triton X-100 and 0.15 µg proteinase K (Roche)] at 55°C. The following day, samples were heat-inactivated for 5′ at 95°C and were centrifuged to remove the debris. Next, 1 µl of the supernatant was used as template DNA in PCR. Templates were checked for the presence of rtTA and/or TRE. Following, PCR mix was used [10× FastStart DNA polymerase buffer with $MgCl_2$ (Roche), 25 mM dNTPs, primers (10 mM), FastStart DNA polymerase (5 U/µl; Roche), sterilized water]. The PCR program consisted of 4 min denaturation at 94°C, followed by amplification through 30 s at 94°C, 30 s at 60°C and 90 s at 72°C and was ended with 5 min at 72°C. PCR products were visualized by adding 10 µl 3× loading mix [30% Orange G (Sigma), 0.2% Gelred (Biotium) in H2O] to 5 µl of the PCR product and separating was done by using gel electrophoresis on a 1.5% agarose gel. Gels were scanned using Gel Doc™ XR+ (Bio-Rad) Molecular Imager with Image Lab™ software.

For validating CGG repeat size, DNA was isolated from the lung tissue as described in the section 'DNA isolation'. The DNA isolates were submitted to a touchdown PCR with Betaine to stretch the secondary structure formed within the expanded repeat and to allow amplification across the CGG repeat (5 M Betaine, primers, 10 mM), 25 mM dNTPs, 10× FastStart DNA polymerase buffer with MgCl2 (Roche), FastStart DNA polymerase (5 U/µl; Roche), sterilized water. The PCR program consisted of an initial denaturation of 10 min at 95°C, followed a touchdown of 70–55°C through 60 s at 95°C, 30 s at 70°C (−1°C/cycle) and 5 min at 72°C, after which the DNA was amplified through 30 cycles of 60 s at 95°C, 60 s at 60°C and 5 min at 72°C, finalized by 10 min at 72°C. PCR products were visualized as described before and were compared with a positive control of known repeat size. Primers used are listed in Supplementary Material, Table S1A.

DNA isolation

Lung tissue was dissected from mice and was put in a 300 µl aliquot of tail mix (50 mM Tris–HCl, pH 7.5, 10 mM EDTA, 150 mM NaCl, 1% SDS and 20 µg proteinase K). Tissue was incubated at 55°C overnight. The next day, 100 µl of 6 M NaCl was added. The sample was shaken and centrifuged at 13.000 rpm (Thermo Scientific; Heraeus Fresco 17 #75002420; Rotor #75003424) for 10 min after which the supernatant was transferred to a new recipient. A 1 ml aliquot of 100% EtOH (ethanol) was added to the supernatant to precipitate DNA and was centrifuged again at 13.000 rpm (Thermo Scientific; Heraeus Fresco 17 #75002420; Rotor #75003424) for 10 min. Supernatant was discarded, and the pellet was rinsed with 500 µl of 70% EtOH. Afterward, the DNA pellet was air-dried and dissolved in 100 µl of sterilized water. The DNA concentration was measured on a NanoDrop™ 2000/2000c spectrophotometer (Thermo Scientific).

Primary hippocampal neuronal culture

Culturing of primary hippocampal neurons was done according to the isolation and culturing procedure described in detail by Seibenhener and Wooten (45). In summary, pregnancies were scheduled using C57Bl/6J mice that are heterozygous hnRNP-rtTA or heterozygous TRE-nCGG-eGFP. A pregnant mouse at 17–19 days post-fertilization was first shortly anesthetized using isoflurane and was euthanized by cervical dislocation. Up to 10 E17-E19 DT embryos for hnRNP-rtTA/TRE-nCGG-eGFP were removed from the uteri and were decapitated under a dissecting microscope after which the hippocampi were carefully isolated and placed in a culture dish with neurobasal medium (Gibco) supplemented with 1% penicillin/streptomycin (Gibco), 1% glutamax (Gibco) and 2% B27-supplement (Gibco). This medium is further referred to as NBM+++. Brain tissues from multiple pups were combined. Hippocampi were dissociated using Trypsin/EDTA. Prior to the dissection procedure, 30 mm glass coverslips were subsequently coated with poly-D-lysine (100 µg/ml; Sigma) overnight or 1 h prior to the procedure followed by laminin (50 µg/ml; Sigma) for at least 30 min. Cells were plated on coated coverslips and were attached to the substrate in a droplet of NBM+++. After 90 min, the volume was adjusted to 2 ml per coverslip in a six well plate, and the plates were stored at 37°C and 5% CO_2. To induce and maintain stable expression of 90 CGG RNA in the primary hippocampal neurons,

2 µl dox (0.5 mM) was administered to the cultures on a regular daily bases for up to 21 days in culture. Daily administration is necessary to ensure the stable induction of the transgene in the primary hippocampal neurons. Since dox is sensitive for light, working solutions of 0.5 mM were prepared and were stored at 4°C in tinted bottles (46).

Compound 1*a* treatment *in vitro*

Analyte 1*a*, specifically 9-hydroxy-5,11-dimethyl-2-(2-(piperidin-1-yl)ethyl)-6H-pyrido[4,3- b]carbazol-2-ium, is a designer, bioactive small molecule RNA-binding probe that shields the expanded CGG repeats by binding the internal GG mismatches preventing RAN translation and the sequestration of proteins to the secondary hairpin-like structure formed by the repeat (42,44). For *in vitro* treatment, compound 1*a* was dissolved in DMSO at a final stock concentration of 2 µM. Each primary hippocampal culture was treated once with compound 1*a*. One microliters of compound 1*a* was added to 2 ml NBM+++ culture medium the same day dox administration started or 1 week after dox induction. Half-life of compound 1*a* was determined in the liver and plasma using HPLC and LC–MS/MS analysis.

Tissue homogenization

Tissues were homogenized in 500 µl of RIPA buffer [20 mM Tris–HCl, pH 7.5, 150 mM NaCl, 1% IGEPAL®, 0.01% sodium dodecyl sulfate (SDS), 1% sodium deoxycholate], containing complete protease inhibitor (Roche), 40 mM beta-mercaptoethanol and 1 µl RNase-OUT (40 U/µl; Invitrogen). Homogenates were incubated for 30 min on ice of which 100 µl was added to 1 ml of TRIzol® reagent (Life technologies) for RNA isolation and the remainder was used for protein isolation.

RNA isolation

Tissue homogenates were made as described in section 'Tissue homogenization'. Hundred microliters of homogenate was added to 1 ml of TRIzol™ reagent (Life technologies) and mixed thoroughly before adding 200 µl of chloroform after which the mix was incubated on ice for 15 min. Samples were spun down at 4°C, 13.000 rpm (Thermo Scientific; Heraeus Fresco 17 #75002420; Rotor #75003424) for 10 min and the aqueous phase of the mix—containing the RNA—was taken and put in a new recipient. To this aqueous phase, one volume of isopropanol was added to precipitate RNA and mixed thoroughly before spinning down again under the same conditions. Pellets were rinsed twice with 80% EtOH and were air-dried. Eventually, the RNA pellets were dissolved in RNase-free water, and the RNA concentration was measured on a NanoDrop™ 2000/2000c spectrophotometer (Thermo Scientific).

Reverse transcriptase quantitative PCR

To measure relative mRNA levels in our samples, we performed reverse transcriptase (RT) quantitative (q) PCR. The RT reaction was performed on 1 µg of RNA using the iScript cDNA synthesis kit (Bio-Rad) according to the manufacturer's instructions. Prior to the RT reaction, a DNase treatment was performed on the samples to remove residual genomic DNA. The qPCR was performed on 0.7 µl of the RT product using iTaq™ Universal SYBR® Green Supermix (ratio, 1:1.5; Bio-Rad) using the CFX96 Touch™ Real-Time PCR Detection System (Bio-Rad). GAPDH2 was used as a reference gene. The PCR program consisted of initial denaturation through 3 min at 95°C, amplification and readout through 40 cycles of 5 s at 95°C, 30 s at 60°C and plate reading, finalized by a melt curve. Primers are listed in Supplementary Material, Table S1A.

Protein isolation

Tissue homogenates were centrifuged at 4°C, 13.000 rpm (Thermo Scientific; Heraeus Fresco 17 #75002420; Rotor #75003424) for 20 min after which a soluble and insoluble fraction were obtained. Of the soluble fraction of the homogenate, the protein concentration was determined with a Pierce™ BCA Protein Assay Kit (Thermo Scientific). Homogenates were diluted to a concentration of 500 µg protein/µl, and a sample loading mix (0.25 M Tris–HCl pH 6.8, 8% SDS, 20% glycerol, 0.008% Bromophenol Blue, 3 M beta-mercaptoethanol) was added to the isolates in a 1:4 ratio and the mixes were heated at 95°C for 5 min. From there on, samples were directly used for further analysis or were stored at −80°C. For FMRpolyG and Rad23b analyses, sample loading mix was immediately added to the soluble fractions after which they were heated and stored for further analyses. Here, the insoluble fraction was also saved and stored at −80°C to determine the amount of these proteins.

Western blot

Western blot analysis was performed to visualize the protein and quantify its relative expression in our samples. Protein was isolated, sample loading mix was added and samples were heated as described in the section 'Protein isolation'. Samples and a protein marker (Precision Plus Protein™ All Blue Standards; Bio-Rad) were run on a 16.5% Criterion pre-cast Tris-Tricine Peptide gel (Bio-Rad) using Tris/Tricine/SDS (TTS) running buffer (Bio-Rad) at 100–150 V. Next, protein was transferred to a 0.2 µm nitrocellulose trans-blot membrane (Bio-Rad) using a Trans-Blot Turbo Transfer System (Bio-Rad). After transfer, the blot was washed briefly with 0.1% Tween 20 in PBS (PBST) and was then blocked for 30′ with 5% milk (Protifar, Nutricia) in PBST. The blot was incubated with primary antibodies diluted in 5% milk/PBST overnight at 4°C. The next day, the blot was rinsed with PBST before incubation with the secondary antibodies. Secondary antibodies were diluted in PBST and were incubated for 60 min at RT. Next, the blot was rinsed with PBST and placed in dH2O. Blots were scanned using a LI-COR Odyssey Imaging System and analysis was performed using LI-COR Odyssey 3.0 software. Antibodies used are listed in Supplementary Material, Table S1B.

Dot blot

To visualize and quantify the proteins that are not found in the soluble fraction of tissue/cell lysates (i.e. proteins in aggregates), we made use of dot blotting. Protein was isolated as described in the section 'Protein isolation', and insoluble fractions were obtained. The insoluble fractions were resuspended in 50–200 µl 20% SDS and were incubated at 95°C for 160 min after which the samples were diluted 3× with 2% SDS. Next, the insoluble fractions were run through a Bio-Dot Microfiltration Apparatus (Bio-Rad) using an Amersham Protran 0.2 µm nitrocellulose membrane (GE Life Sciences). Prior to loading the samples, the membrane was washed with 20 and 2% SDS, respectively, and once more with 2% SDS after running the samples. Afterward, the blot was blocked in 5% milk/PBS for 30 min and incubated with a primary antibody diluted in 5% milk/PBS overnight at 4°C. The

following day, the blot was rinsed with PBS and incubated with a secondary antibody diluted in PBS at RT for 60 min. Next, the blot was rinsed again with PBS and placed in dH2O. Blots were scanned using a LI-COR Odyssey Imaging System, and analysis was performed using LI-COR Odyssey 3.0 software. To normalize for the amount of input on the dot blot, the soluble fractions accompanying the insoluble fractions used were processed for Western blot analysis as described in the section 'Western blot' and were stained against a loading control (cofilin). Antibodies used are listed in Supplementary Material, Table S1B.

Determination of 1*a* concentration in liver samples

Tissue samples were flash-frozen, shipped on dry ice and stored at −80°C until analyzed. Samples were thawed on ice and homogenized in three times w:v water. Liver homogenate was mixed 1:3 with acetonitrile containing 100 nM carbamazepine as an internal standard. The sample was allowed to sit on ice for 30 min to precipitate proteins prior to filtration using a MultiScreen Solvinert 0.45 µm low-binding hydrophilic PTFE plate (Millipore). The filtrate was directly analyzed by LC–MS/MS using a Thermo BetaSil column, 2.1 × 50 mm, 5 µm. The analyte 1*a* was detected on a Sciex 5500 mass spectrometer following mass transition Q1 = 375.1 AMU and Q2 = 84.2 AMU. Samples were compared with freshly prepared standards prepared in blank mouse liver homogenates. Concentration was determined as ng analyte per mg liver tissue. Density = 1 was assumed to convert to molarity (1 mg = 1 µl). Half-life of compound 1*a* was determined in the liver and plasma using HPLC and LC–MS/MS analysis.

Immunological staining

Tissues were fixed overnight in 4% paraformaldehyde (PFA) at 4°C and were embedded in paraffin according to in-house protocols. Sections of 6 µm were cut and placed on silane-coated slides (Klinipath). The sections were deparaffinized in decreasing concentrations of alcohol, starting with xylene and ending in dH_2O, before performing antigen retrieval by microwave treatment in 0.01 M sodium citrate (pH 6). For immunohistochemical staining using DAB, endogenous peroxidase activity was blocked with 0.6% H2O2 in PBS. For fluorescent staining, sections were blocked in Sudan Black. When staining for FMRpolyG, an additional incubation step with proteinase K (5 µg/ml) was performed for 20–30 min at 37°C. Immunostaining was performed overnight at 4°C with primary FMRpolyG antibodies diluted in PBS/0.5% milk/0.15% glycine (PBS+). Staining with secondary antibodies was performed at RT for 60 min. For immunohistochemical staining using DAB, antigen–antibody complexes were visualized using DAB substrate (DAKO) after which the slides were counterstained with hematoxylin for 5 min and subsequently mounted with Entellan (Merck Milipore International). Fluorescent stained slides were mounted using ProLong™ Gold with DAPI (Invitrogen). Antibodies used are listed in Supplementary Material, Table S1B.

Fluorescence microscopy

All fluorescent imaging presented in this study was performed using a Leica TCS SP5 confocal microscope with a 20× lens. Filters used: 405 nm (Hoechst/DAPI), 488 nm argon laser (Alexa 488/GFP), 561 nm (Cy3) and 633 nm (Cy5). ImageJ image analysis software was used to process the images.

Quantification of inclusions

Inclusions were quantified by first counting approximately 100 GFP-positive cells and then by counting the number of FMRpolyG- and ubiquitin-positive intranuclear inclusions in these GFP-positive cells from different aged dox-treated primary hippocampal neuronal cultures using a Leica confocal microscope and LAS AF software. After administration of compound 1*a*, the same measurement principle was applied, only this time, mainly focusing on FMRpolyG-positive intranuclear inclusions.

The number and size of inclusions in the liver tissue was determined using an Olympus BX40 microscope and CellSens Dimension software. Inclusions were quantified by counting liver cells at a 40× magnification in five randomly selected areas per liver slice. FMRpolyG-positive or inclusions were quantified using a counting frame. Per mouse, two liver slices were counted and then the average of both counts was used. Researchers were blinded for experimental groups. The same quantification procedure was also applied for Rad23b-positive inclusions.

Statistical analysis

Statistical analysis was performed using GraphPad Prism software version 8 (47). Statistical test used for *in vitro* experiments is the one-way ANOVA multiple comparison test. For statistical analysis between the *in vivo* experimental groups, one-way ANOVA test followed by Tukey's *post hoc* correction test was used. A *P*-value of $P < 0.05$ was considered significant.

Results

Intranuclear inclusions in an inducible neuronal cell model for FXTAS

Previously, we showed that the formation of intranuclear inclusions in an inducible mouse model of FXTAS was reversible by stopping the expression of RNA containing the expanded CGG repeat (36). After this proof of principle, the next challenge was to find a therapeutic intervention targeting the pathogenic trigger for FXTAS, the *FMR1* RNA containing a CGG_{exp}. To test potential therapeutic interventions, we generated inducible hippocampal neuronal cultures derived from inducible DT TRE-nCGG-eGFP/hnRNP-rtTA mice. In these cells, either the RNA bearing the 5′UTR of the *FMR1* gene with a control size repeat of 11 CGGs or RNA containing the 5′UTR of the *FMR1* gene with a PM size of 90 CGGs was coupled to eGFP. These cultures were derived from E17-19 embryos from timed breedings with heterozygous transgenic mice. This resulted in a mixed population of nCGG-GFP RNA-positive and -negative cells. Indeed, administration of dox to the culture medium resulted in GFP-positive and GFP-negative cells in cultures originating from both 11 CGG and 90 CGG repeat containing mice (Fig. 1A, A–F). There were no GFP-positive cells in cultures originating from DT mice without the addition of dox to the culture medium (Fig. 1A, G–L) or in control cultures containing only one of the two transgenes (not shown).

To confirm whether intranuclear inclusions could be formed in these primary hippocampal neuronal cell cultures, we performed immunofluorescence (IF) staining for ubiquitin. Ubiquitin-positive inclusions were observed in GFP-positive cells in TRE-90 CGG-eGFP/hnRNP-rtTA cultures after 10 days of dox induction. The number of ubiquitin-positive intranuclear inclusions increased significantly in time up to 37% of the GFP positive cells at 24 days of dox induction (Fig. 1B and C). In addition, previous work demonstrated that ubiquitin and FMRpolyG co-localize in inclusions in transfected cells, brain

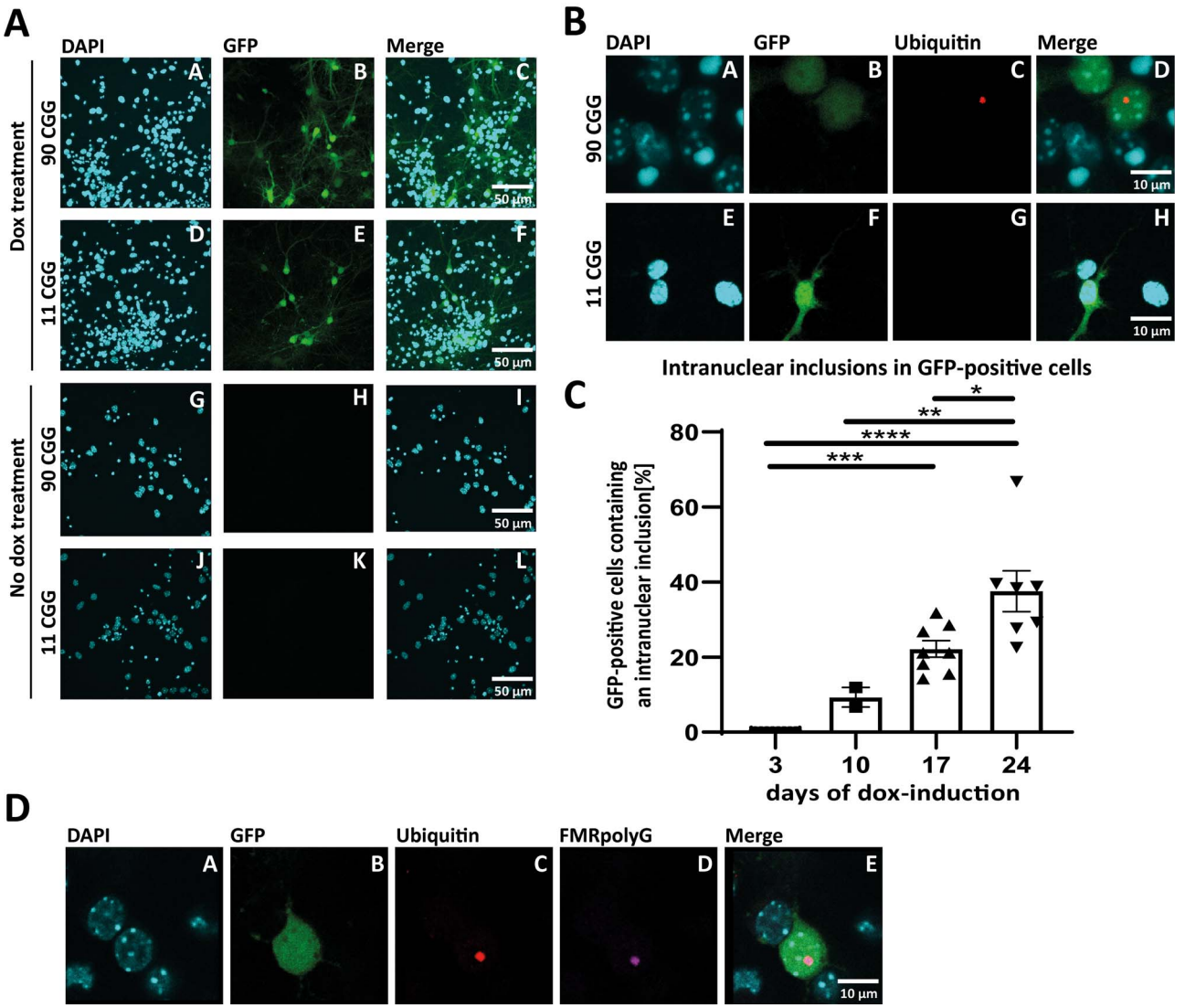

Figure 1. FMRpolyG-positive inclusions form in GFP-positive primary hippocampal neurons. (**A**) eGFP expression (green) after dox induction of 11CGG and 90CGG double transgenic (DT) TRE-nCGG-eGFP/hnRNP-rtTA primary hippocampal neurons. No eGFP expression is observed in DT neuronal cultures without dox. (**B**) Ubiquitin-positive intranuclear inclusions (red) are found in GFP-positive TRE-90CGG-eGFP/hnRNP-rtTA cells, but not in GFP-positive TRE-11CGG-eGFP/hnRNP cells or GFP-negative cells. (**C**) Quantification of intranuclear inclusions in GFP-positive cells. The percentage of GFP-positive nuclei containing GFP-positive inclusions after 0 ($n=8$), 10 ($n=2$), 17 ($n=8$) and 24 ($n=7$) days dox treatment. Per isolation and per timepoint, 100 GFP-positive cells were counted. For statistical analysis, the one-way ANOVA test with multiple comparison was used. Error bars represent standard error of the mean (SEM). Asterisks indicate different levels of significance ($^{*}P \leq 0.05$, $^{**}P \leq 0.01$, $^{***}P \leq 0.001$ and $^{****}P < 0.0001$). (**D**) Co-localization of ubiquitin (red) with FMRpolyG (purple) in intranuclear inclusions. Approximately, 90% of ubiquitin-positive and FMRpolyG-positive intranuclear inclusions co-localize.

tissue of mouse models and post-mortem brain tissue from FXTAS patients (10,29,36). IF double staining confirms that, in inducible hippocampal mouse neurons, ubiquitin and FMRpolyG co-localize within approximately 90% of all intranuclear inclusions (Fig. 1D).

To study which cell types are present in the neuronal culture, we performed IF double staining in the primary hippocampal cell cultures. We found that both neurons and astrocytes are present in the primary hippocampal cultures using the neuronal marker microtubule-associated protein 2 (MAP2) and the astrocytic marker glial fibrillary acidic protein (GFAP), respectively (Fig. 2A and B). More specifically, antibodies against Ca^{2+}-/calmodulin-dependent protein kinase II (CamKII) and gamma-aminobutyric acid (GABA) for different types of neurons showed that both excitatory and inhibitory neurons can be found in these primary hippocampal cultures (Fig. 2C and D). Intranuclear inclusions were only found in GFP-positive neurons but not in astrocytes (Fig. 2A–D). In short, these data confirm that we generated an *in vitro* neuronal culture with multiple cell types and that these primary hippocampal neurons are capable of forming ubiquitin-positive and FMRpolyG-positive intranuclear inclusions, which is the major neuropathological hallmark for FXTAS.

Compound 1*a* can reduce number of FMRpolyG-positive inclusions in primary neurons

Since the primary hippocampal cultures showed one of the main hallmarks of the disease, we could use the model to test the therapeutic interventions that may halt or reduce the formation

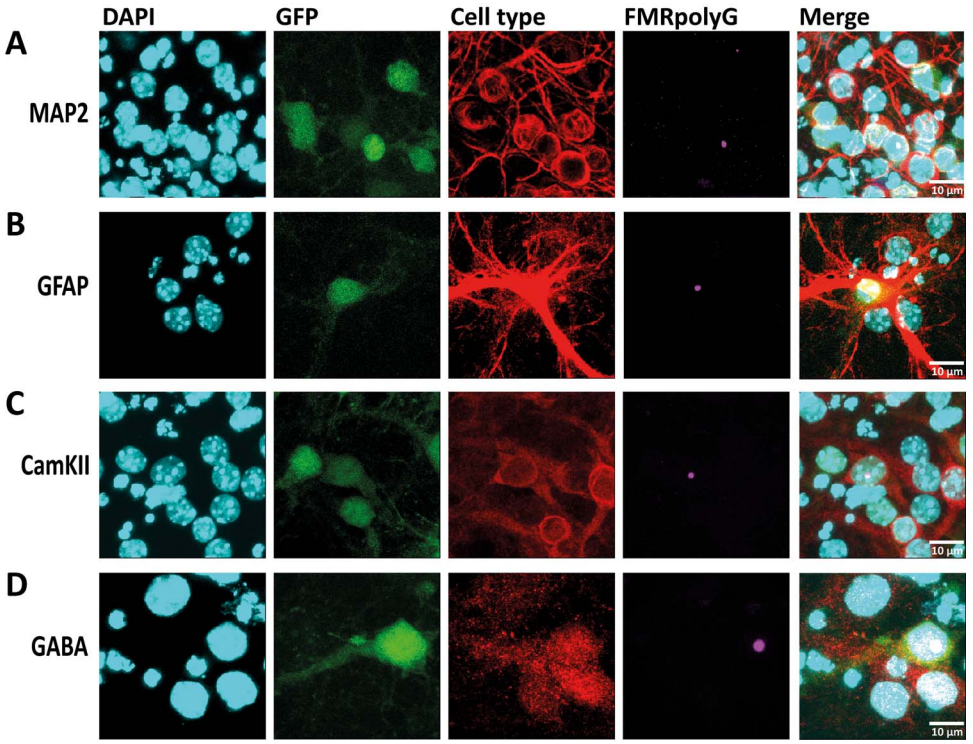

Figure 2. Multiple relevant cell types formed in an *in vitro* neuronal model for FXTAS. Immunofluorescent staining using the (**A**) neuronal MAP2 and (**B**) astrocytic GFAP markers show that these *in vitro* cultures are heterogenous. More specifically, immunofluorescent staining shows that both (**C**) inhibitory and (**D**) excitatory neurons are present in the cultures, and in both types of neurons, FMRpolyG-positive intranuclear inclusions are formed. FMRpolyG-positive intranuclear inclusions were not present in astrocytes. Scale bars represent 10 µm.

of FMRpolyG-positive inclusions. Several small chemical compounds that target CGG_{exp} were developed of which compound 1*a* was a promising candidate (Fig. 3A). It can bind to the internal GG mismatches of the expanded CGG repeat shielding the RNA and thus prevent its translation (42). For several repeat-associated disorders, several promising compounds have been described [reviewed in (43)].

Compound 1*a* was first tested for toxicity. Titration experiments showed that using concentrations of 1 and 10 nM of compound 1*a* did not result in abnormal cell death and that compound 1*a* did not result in adverse effects in the culture up to 24 days after the compound administration. Also, using HPLC and LC–MS/MS analysis, we calculated the half-life of compound 1*a* in blank NBM+++ to be 9 h. Next, we performed IF staining, and the number of FMRpolyG-positive intranuclear inclusions was quantified. Figure 3B represents a schematic overview of the dox and compound 1*a* treatment. We added compound 1*a* 1 day prior to the start of dox induction followed by 17 days of dox treatment. Upon quantification, significantly less intranuclear inclusions were observed with both 1 and 10 nM concentrations of compound 1*a* (Fig. 3C). The addition of compound 1*a* 1 week after the start of dox induction resulted also in a significant reduction of the number of intranuclear inclusions compared with untreated cultures (Fig. 3D). There was no significant difference in the number of inclusions between cultures that received 1*a* prior to the dox induction and 1 week after dox induction. In summary, these data show that compound 1*a* is capable of reducing the number of FMRpolyG-positive intranuclear inclusions in primary hippocampal neuronal cultures when applied as a preventative treatment and when administered after the CGG repeat RNA expression is induced in these primary neurons.

Inducible ubiquitous expression of expanded CCG RNA in mice

To confirm the results from the *in vitro* study in an animal model, we injected compound 1*a* in this ubiquitous inducible mouse model (40). These mice show ubiquitous expression of a CGG_{exp}, resulting in the rapid formation of inclusions in the liver but not in the brain.

To induce transgene expression in DT mice, we provided them with dox or sucrose–water from the ages of P24 to 27. Mice were then split into five experimental groups, as shown in Figure 4A. All mice were DT mice except for group 3, which had only one of the two transgenes. Group 1 was the negative control group in which mice were left untreated for both dox and compound 1*a*. Group 2 was the compound control group where mice only received a single IP injection of compound 1*a* to account for the effects compound 1*a* has on these mice. Group 3 comprised single transgenic mice having only the hnRNP-rtTA transgene. These mice were provided with only dox to account for any leakage of the promoter. Group 4 was the positive control and was administered dox to induce expression of the transgene, but the mice were not treated with compound 1*a*. Finally, group 5 was the treatment group. These mice were provided with dox in their drinking water followed by a single IP injection of compound 1*a*. After 5 days, all mice showed a normal increase in body weight (Supplementary Material, Fig. S1A) and the expression of the transgene was confirmed for dox-induced DT mice through quantitative RT-PCR of the expanded CGG mRNA (Fig. 4B) and immunohistochemical staining for GFP (Fig. 4C) on the liver tissue. Sucrose–water and single transgenic control mice showed no expression of the expanded CGG mRNA and no staining of GFP in liver tissue (Fig. 4B). Western blot

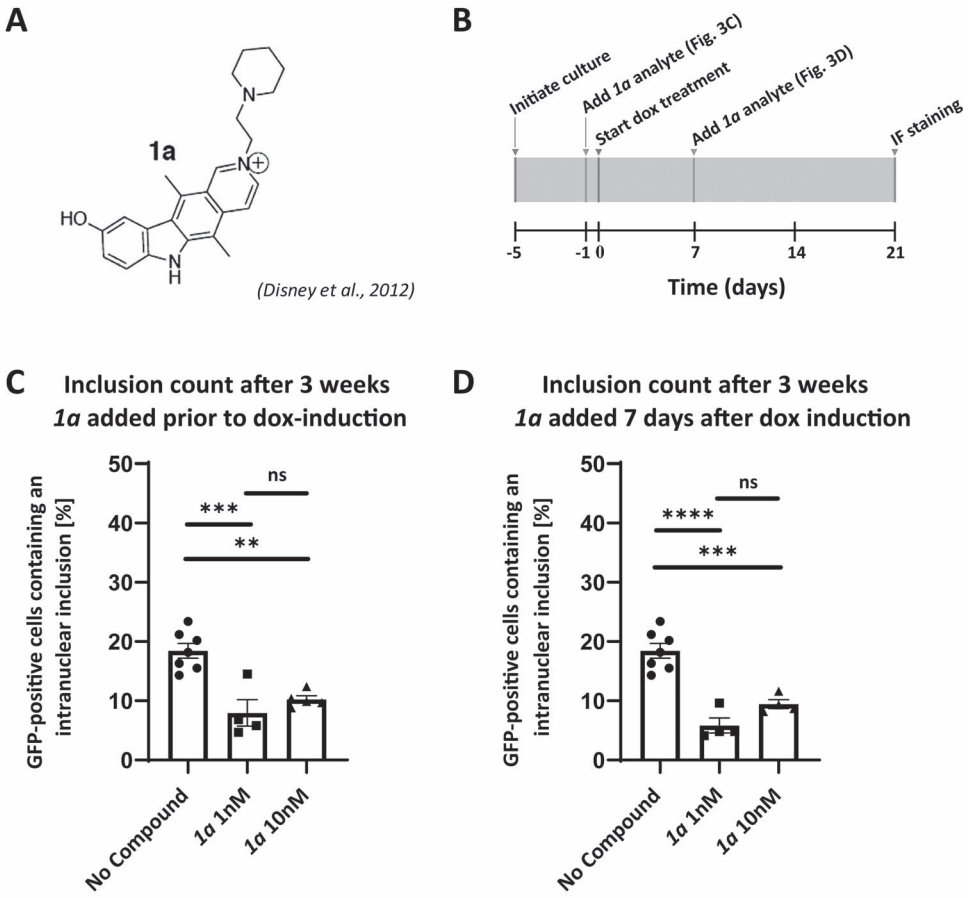

Figure 3. Less FMRpolyG-positive intranuclear inclusions *in vitro* after treatment with 1*a*. (**A**) Chemical structure of compound 1*a*. (**B**) Schematic overview of doxycycline and compound 1*a* treatment. Compound 1*a* was added 1 day prior to the start of doxycycline induction followed by (**C**) 21 days of doxycycline treatment. Significantly less intranuclear inclusions were observed with a concentration of both 1 nM ($n = 4$; $P \leq 0.001$) and 10 nM ($n = 5$; $P \leq 0.01$) of compound 1*a*, both compared with no compound treatment ($n = 7$). No significant difference was found between the concentrations of 1 and 10 nM used for compound 1*a*. (**D**) Addition of compound 1*a* 7 days after start of doxycycline induction resulted also in a reduction of the number of intranuclear inclusions for 1 nM ($n = 4$; $P < 0.0001$) and 10 nM ($n = 4$; $P \leq 0.001$) of compound 1*a* compared with untreated cultures ($n = 7$). No significant difference was found between the concentrations of 1 nM and 10 nM used for compound 1*a*. No significant difference was observed in the number of intranuclear inclusions between cultures that received compound 1*a* (both 1 and 10 nM) prior to the doxycycline induction and cultures that received compound 1*a* after 7 days of dox induction. For statistical analysis, the one-way ANOVA test with multiple comparison was used. Asterisks in the figures indicate different levels of significance (**$P \leq 0.01$, ***$P \leq 0.001$ and ****$P < 0.0001$). Error bars represent SEM.

analysis further confirmed the expression of GFP protein in the liver (Fig. 4D; full blots in Supplementary Material, Fig. S2). Expression of expanded CGG mRNA and GFP protein was limited to transgenic mice induced with dox and was absent in non-DT and negative control mice. No significant differences were observed in these levels between mice treated with compound 1*a* or vehicle (DMSO) (Fig. 4B and D). After weighing the mice daily and sacrificing the mice and macroscopically observing the liver, severe liver toxicity was absent in these experiments (Supplementary Material, Fig. S1A and B). To confirm there was no liver toxicity present, we performed quantitative RT-PCR on mRNA from the livers of positive (untreated DT and treated DT mice) and negative control mice for glutathione peroxidase-1 (GPX-1) and cytochrome C (CytC), which are indicative for mitochondrial stress when elevated in the liver (Supplementary Material, Fig. S1C and D). Indeed, both GPX-1 and CytC mRNA levels were similar in dox-induced and control mice, confirming absence of severe liver toxicity in these DT mice. In summary, these data show that we successfully induced the expression of the transgene at the mRNA and protein levels without any severe toxicity after 5 days.

Double transgenic mice produce FMRpolyG-positive protein inclusions that deplete upon treatment with 1*a*

Having confirmed the expression of the transgene in these mice, the next step was to see whether expression leads to the formation of intranuclear inclusions, which is the pathological hallmark for FXTAS. For the first time, we could show, through immunohistochemistry staining in the liver sections for FMRpolyG, the presence of FMRpolyG-positive inclusions in dox-induced DT mice but not in the sucrose–water or single transgenic control groups (Fig. 5A). FMRpolyG-positive inclusions were located both in the cytoplasm and in the nucleus, as opposed to FXTAS-patient brain tissue where the inclusions are primarily intranuclear (7,8). In addition to FMRpolyG-positive inclusions, we also confirmed the presence of ubiquitin-positive inclusions in the liver tissue from dox-induced DT mice (Fig. 5B). Co-localization of both ubiquitin and FMRpolyG within the inclusions was confirmed through IF double labeling of the liver sections (Fig. 5C; negative control shown in Supplementary Material, Fig. S3A). Having confirmed the expression of the transgene and the presence of FMRpolyG-positive inclusions, we next tested whether treatment with compound 1*a* could reduce the

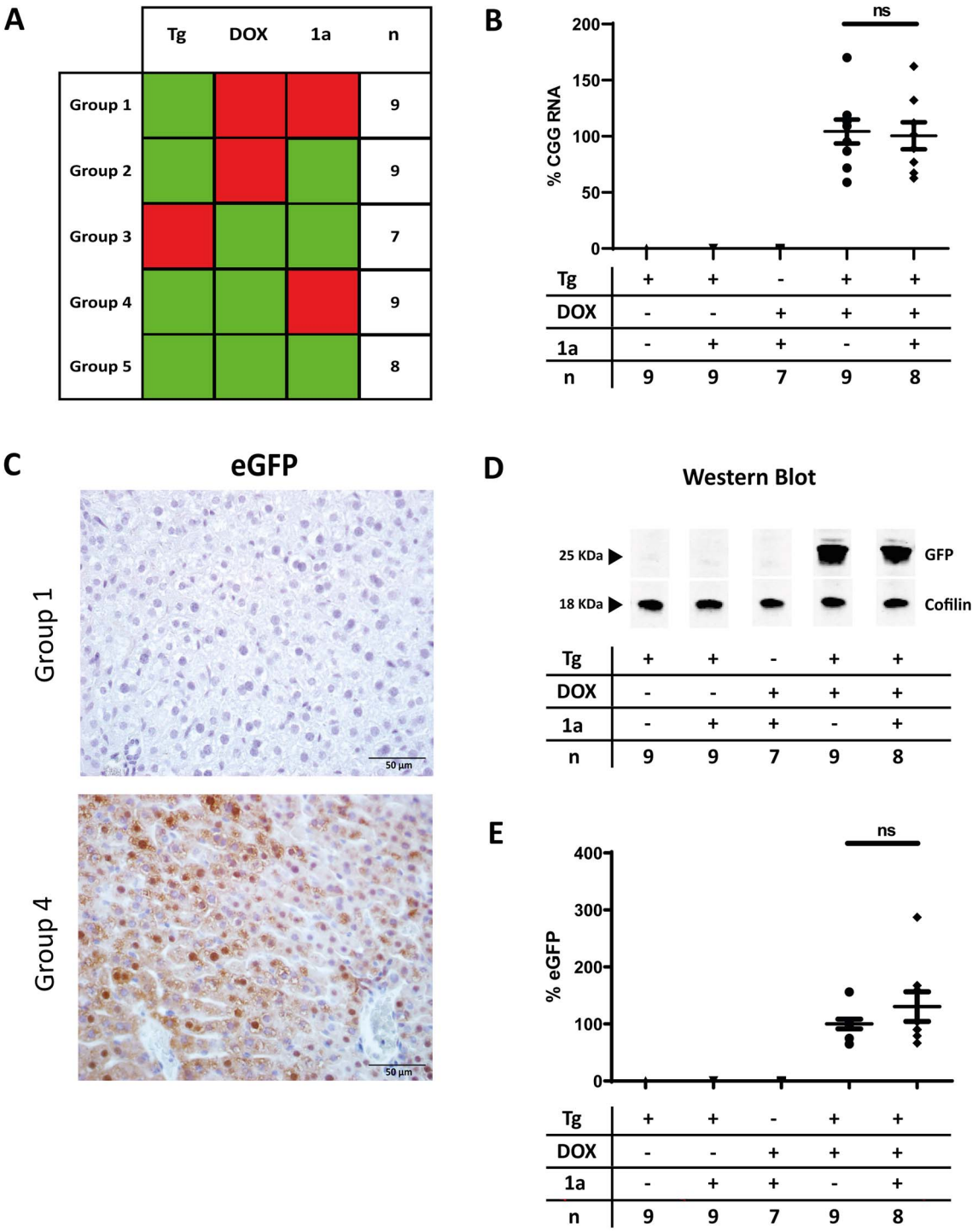

Figure 4. *In vivo* induction of expanded CGG repeat expression in DT mice. (**A**) Schematic overview of experimental mouse groups in regard to transgenic status (Tg), doxycycline (dox) administration, compound 1*a* administration and group size (*n*). (**B**) Relative expression level of 90CGG mRNA analyzed through quantitative RT-PCR. Only the dox-induced DT mice express the expanded repeat mRNA. Values are shown as percentage relative to the positive control group (group 4). No significant difference in 90CGG mRNA expression between the compound 1*a* untreated and treated DT group was found (one-way ANOVA *post hoc* Tukey's). Error bars represent standard deviation (SD). (**C**) Immunohistological staining against eGFP in liver tissue of group 1 (negative control; upper image) and group 4 (positive control; lower image) mice. 40× magnification. Scale bars represent 50 µm. Group 1 shows no staining, whereas group 4 shows a strong staining throughout the tissue. (**D**) Western blot analysis of eGFP protein expression across experimental groups. Upper lane shows eGFP at 25KDa. Lower lane shows loading control cofilin at 18 KDa. Only the dox-induced DT mice express GFP protein. Full western blot in supplements (Supplementary Material, Fig. S2). (**E**) Relative expression of eGFP protein analyzed through western blot. Values are shown as percentage relative to the positive control group (group 4). There is no significant difference in eGFP protein expression between the compound 1*a* untreated and treated DT mice (one-way ANOVA *post hoc* Tukey's). Error bars represent SEM.

number of FMRpolyG-positive inclusions and FMRpolyG levels *in vivo*. Before onset of the study, we determined the half-life of compound 1*a* in the liver and plasma at 32 and 5 h, respectively. This is important to understand the effectiveness of compound 1*a* after a single IP dosing regimen. First, we quantified the number of FMRpolyG-positive inclusions in all the experimental groups after treatment with compound 1*a* (quantification method is discussed in the section 'Quantification of inclusions'). We did not find a significant decrease for the number of FMRpolyG-positive inclusions between the dox-induced positive control and 1*a*-treated DT mice (Fig. 5D; $P = 0.1407$). To have a more accurate measure of the amount of FMRpolyG protein present in the tissue of these mice, we used the dot blot technique to visualize the amount of FMRpolyG within the insoluble fractions of protein lysates taken from the liver tissues. Owing to the localization of FMRpolyG within aggregates, it is unfortunately not possible to detect the protein in the soluble fractions on a western blot. Using the dot blot technique to visualize the FMRpolyG protein levels within the insoluble fractions of protein lysates, we observed a significant decrease of FMRpolyG–protein levels after treatment with compound 1*a* (Fig. 5E; $P < 0.001$; full blots shown in Supplementary Material, Fig. S4).

Another protein commonly observed to be present within the inclusions in the brain tissue from FXTAS patients is RAD23B, a protein involved in the ubiquitin-mediated proteasomal degradation pathway (36,38,48). Indeed, Rad23b-positive inclusions could be detected in the dox-induced DT mice as well (Fig. 6A). Notably, in sucrose–water, control mice Rad23b was localized only in the cytoplasm without the formation of aggregates. IF staining confirmed co-localization of Rad23b-positive and FMRpolyG-positive inclusions, both in the cytoplasm and nucleus (Fig. 6B; negative control shown in Supplementary Material, Fig. S3B). All together, these data show that expression of CGG_{exp} mRNA resulted in the formation of FMRpolyG-positive inclusions intranuclearly as well as cytoplasmic. We could also confirm the presence of Rad23b-positive intranuclear and cytoplasmic inclusions. Rad23b co-localized in the vast majority of inclusions nicely with FMRpolyG. The presence of Rad23b in these inclusions suggests a role for the proteasome degradation pathway in inclusion formation. Similarly, we quantified the number of Rad23b-positive inclusions and aggregated the protein levels. Interestingly, dox-induced DT mice treated with compound 1*a* showed less Rad23b-positive inclusions compared with control dox-induced DT mice (Fig. 6C; $P < 0.01$). Also, Rad23b protein level from the insoluble protein fractions was significantly decreased in DT mice treated with compound 1*a* (Fig. 6D; $P < 0.01$; full blots shown in Supplementary Material, Fig. S5).

Discussion

This study shows the strength of the ubiquitous expression inducible model in the rapid screening of potential therapeutic interventions targeting cellular toxicity. The *in vitro* primary hippocampal neuronal culture serves as a primary screening to identify promising therapeutics in a relevant cell type. The *in vivo* mouse model confirms the potential therapeutic effect of compound 1*a* on FMRpolyG-positive inclusions and the FMRpolyG protein level in liver tissue. Although liver tissue is not affected in FXTAS, we believe the *in vivo* model can serve as a quick *in vivo* screening method to study therapeutic strategies to prevent cellular toxicity. In contrast to other FXTAS mouse models, this mouse model shows early manifestations, including FMRpolyG-positive inclusions. To our knowledge, we are here first to report the use of a small chemical compound, specifically compound 1*a*, in a ubiquitous inducible mouse model. We were able to induce FMRpolyG inclusion formation in the primary hippocampal neuronal cultures and, upon treatment with compound 1*a*, significantly decrease the number of FMRpolyG-positive inclusions *in vitro*. Additionally, we have successfully induced the formation of FMRpolyG-positive inclusions in the liver tissue of the inducible mouse model. Unfortunately, we were not able to reduce the FMRpolyG-positive inclusions in liver tissue, but we showed that compound 1*a* could reduce insoluble FMRpolyG protein levels by targeting the CGG_{exp} mRNA in the ubiquitous inducible mice. We successfully generated a relevant primary neuronal cell culture model derived from the inducible mouse model displaying FXTAS-related neuropathology in all cells, allowing the rapid screening of future targeted interventions *in vitro* and to confirm their potential *in vivo*.

Cellular and animal models have significantly contributed to the understanding of the underlying molecular mechanisms of FXTAS. Recently, our group demonstrated that reversibility of both neuropathology and functional deficits in an inducible FXTAS mouse model could be achieved (36). With this work, we demonstrated that effective targeted treatment for patients with FXTAS might be possible.

The challenge in the search for therapeutic interventions is to develop a rapid and reliable drug screening model. In the present study, we present a relevant cellular model and *in vivo* mouse model for rapid testing of potential therapeutic interventions (40). We were able to successfully induce the formation of FMRpolyG-positive inclusions in these *in vitro* and *in vivo* models, and subsequently, significantly reduce FMRpolyG-positive inclusions *in vitro* and FMRpolyG protein levels *in vivo* through targeting the CGG_{exp} using the small molecule, 1*a*. Because of the rapid development of relevant pathologies, in contrast to other PM mouse models where FXTAS-related pathologies develop only after months, both *in vitro* and *in vivo* models are suitable for rapid determining of the therapeutic potential of targeted interventions against the CGG_{exp}.

In vitro, we were able to show that dox induces the expression of GFP and thus CGG_{exp} mRNA in primary hippocampal neuronal cultures without any leakage of the Tet-On system. Heterozygous hnRNP-rtTA mice were crossed with heterozygous TRE-nCGG-eGFP mice resulting in 25% of the offspring having both transgenes. After administration of dox to the culture medium, approximately, 25% of the neurons show GFP expression, as expected by Mendelian inheritance. Primary neuronal cell cultures from the hnRNP-rtTA/TRE-90 CGG-eGFP mice show the presence of characteristic intranuclear inclusions in both neurons (excitatory and inhibitory) and astrocytes, illustrating similarities between this model and the post-mortem brain tissue from FXTAS patients (8). Interesting to note is that primary neurons cultured from the Dutch KI mouse model showed no inclusion phenotype at all. This is presumably owing to the fact that this mouse model uses an endogenous *FMR1* promoter resulting in lower expression (data not shown). Since FXTAS is a late onset disorder, the process of inclusion formation needs time. Therefore, to study the potential of therapeutic interventions such as 1*a* on inhibiting inclusion formation, an overexpression *in vitro* model is necessary. We also generated cultures of FXTAS patient fibroblasts and mouse embryonic fibroblasts (MEFs) from the inducible mice. In both models, we also could not observe inclusion formation in time (data not shown).

Ubiquitin-positive intranuclear inclusions in neurons and astrocytes are the neuropathological hallmark of FXTAS. The formation of inclusions staining positive for both ubiquitin and

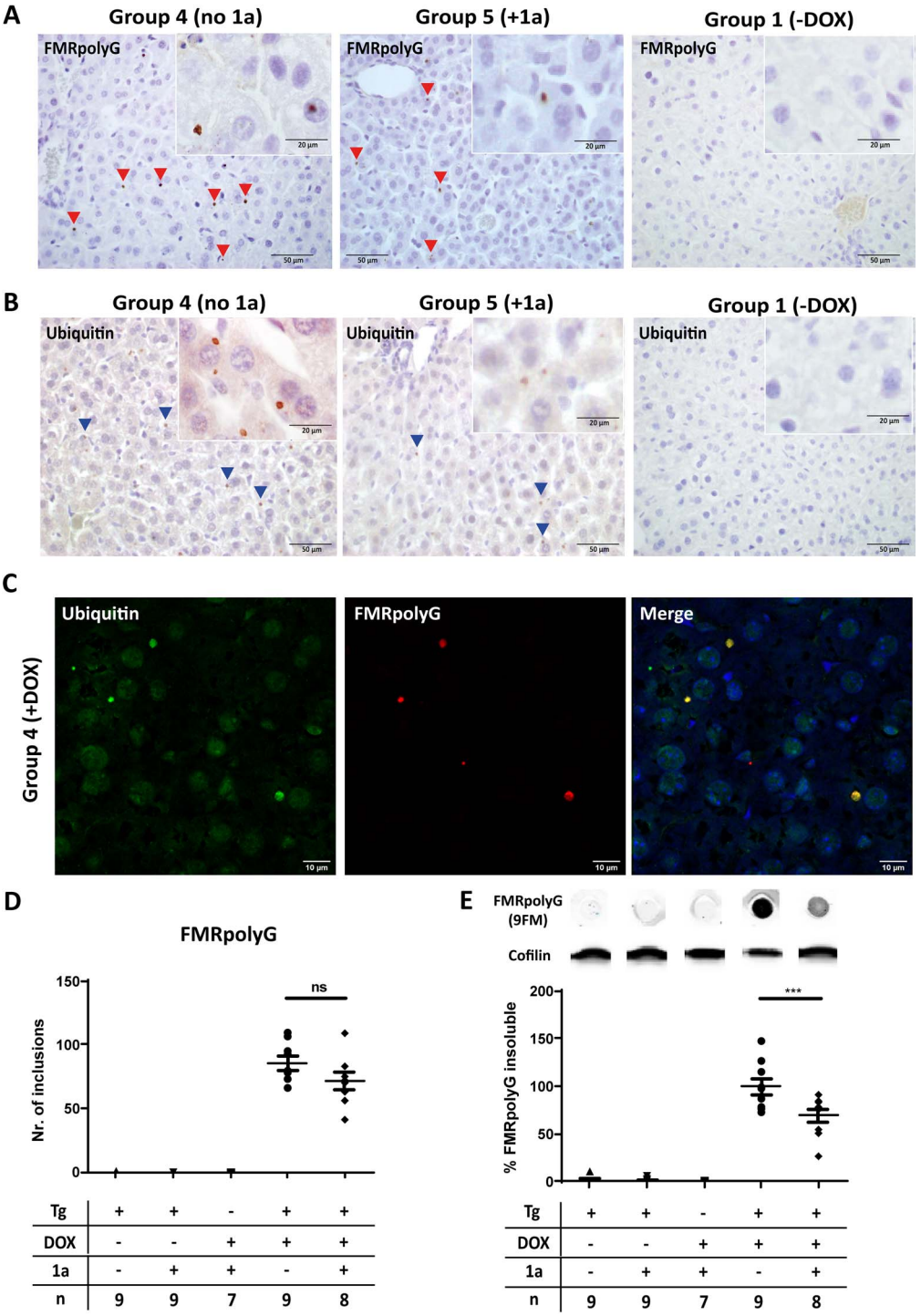

Figure 5. Dox-induced DT mice form FMRpolyG-positive inclusions that co-localize with ubiquitin. Treatment with compound *1a* depletes inclusions and insoluble FMRpolyG protein levels. (**A**) Immunohistological staining of liver tissue belonging to, respectively, compound *1a* untreated DT (group 4), treated DT (group 5), and negative control mice (group 1) for FMRpolyG. Magnifications used are 40× and 100× for inset. Scale bars represent 50 and 20 µm for inset. Red arrowheads show FMRpolyG-positive inclusions. **(B)** Immunohistological staining of liver tissue belonging to, respectively, compound *1a* untreated DT (group 4), treated DT (group 5), and negative control (group 1) mice for ubiquitin. Magnifications used are 40x and 100x for inset. Scale bars represent 50 µm and 20 µm for inset. Blue arrowheads show ubiquitin-positive inclusions. (**C**) Immunofluorescent double staining of liver tissue of compound *1a* untreated DT (group 4) mice for FMRpolyG (red) and ubiquitin (green). Magnification used is 100×. Scale bars represent 10 µm. Merged images show co-localization of FMRpolyG and ubiquitin within inclusions. (**D**) Quantification of number of FMRpolyG-positive inclusions found in liver tissue. There is no significant decrease in inclusion count upon treatment with compound *1a* (one-way ANOVA *post hoc* Tukey's). (**E**) Quantification of insoluble FMRpolyG levels present in liver tissue using the dot blot. Cofilin analyzed through western blot is depicted as a loading control. Full blots in supplements (Supplementary Material, Fig. S4). Insoluble FMRpolyG (9FM) signal was calculated using the cofilin signal as loading control. There is a significant decrease of insoluble FMRpolyG upon treatment with compound *1a* (one-way ANOVA *post hoc* Tukey's; $P < 0.001$). Error bars in this figure represent SEM. Asterisks indicate different levels of significance (***$P \leq 0.001$).

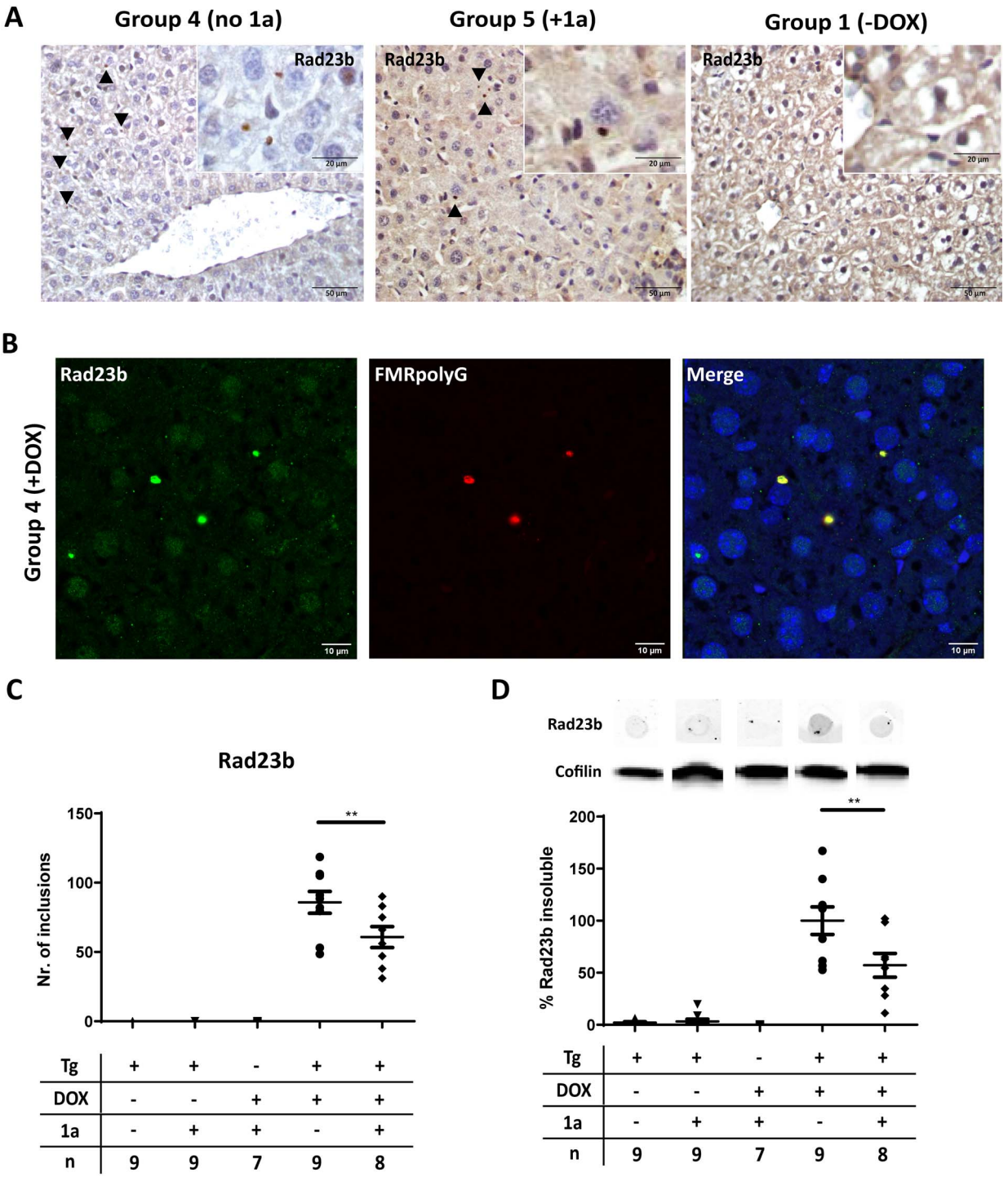

Figure 6. Dox-induced DT mice form Rad23b-positive inclusions that co-localize with FMRpolyG. Treatment with compound *1a* depletes these inclusions as well as insoluble Rad23b protein levels. (**A**) Immunohistological staining of liver tissue belonging to, respectively, compound *1a* untreated DT (group 4), treated DT (group 5) and negative control mice (group 1) for Rad23b. Magnifications used are 40× and 100× for inset. Scale bars represent 50 and 20 µm for inset. Black arrowheads show protein inclusions. (**B**) Immunofluorescent double staining of liver tissue belonging to compound *1a* untreated DT (group 4) against FMRpolyG (red) and Rad23b (green). Magnification used is 100×. Scale bars represent 10 µm. Merged images show co-localization of FMRpolyG and Rad23b within inclusions. (**C**) Quantification of number of Rad23b-positive inclusions found in liver tissue. There is a significant decrease in inclusion count upon treatment with compound *1a* (one-way ANOVA *post hoc* Tukey's; $P < 0.01$). (**D**) Dot blot analysis of insoluble Rad23b present in liver tissue. Cofilin analyzed through western blot is depicted as a loading control. Full blots in supplements (Supplementary Material, Fig. S5). Insoluble Rad23b signal was calculated using the cofilin signal as loading control. There is a significant decrease of insoluble Rad23b upon treatment with compound *1a* (one-way ANOVA *post hoc* Tukey's; $P < 0.01$). Error bars in this figure represent SEM. Asterisks indicate different levels of significance ($^{**}P \leq 0.01$ and $^{***}P \leq 0.001$).

FMRpolyG, together with the presence of these inclusions in both neurons and astrocytes, like in post-mortem brain from patients with FXTAS, points toward an appropriate *in vitro* model to further test possible therapeutic interventions for FXTAS.

From previous work, we know that these mice exposed to dox may experience quick deterioration of their condition owing to liver toxicity and die after 5 days (40). Therefore, these mice form a useful model for quick testing of general cellular toxicity. Although the brain is the organ of interest in FXTAS, in this model, the study of inclusion formation seems not to be possible in the brain since the expression of the CGG_{exp} RNA can never be long enough because the mice die after only 4 days of dox treatment. Other pathogenic triggers, such as deficient mitochondrial signaling, may also contribute to the dramatic cellular toxicity observed that the mice die before any formation of inclusions in the brain or any other organ. Another possible explanation why these mice do not have expression in the brain is that dox may need more time to reach the brain and to induce the transgene expression in the brain. Because of this previously observed phenotype in the liver, we chose to use liver tissue for further analyses.

Although the primary scope of this study was the effect of compound *1a* on the production of FMRpolyG and the formation of inclusions, the role of these inclusions should not be left undiscussed. The presence of significant numbers of inclusions in several brain regions in both neurons and astrocytes suggests that such inclusions are a common neuropathological correlate of the tremor and ataxia phenotype seen in FXTAS patients and PM carriers (8). In analogy with FXTAS patients, ubiquitin-positive intranuclear inclusions can also be detected in the brains of the Dutch CGG-KI mice (37). Cognitive and behavioral deficits in these mice correlate nicely with the increased number of intranuclear inclusions found in both neurons and astrocytes (49). Recently, we published about a new *Gfa2* mouse model with astroglial-specific expression of the CGG_{exp} RNA throughout the entire brain, including cerebellar Bergmann glia. We could show that astrocyte-specific expression of the CGG_{exp} RNA is sufficient to induce key features of FXTAS pathology, including RAN translation of the FMRpolyG protein, the formation of ubiquitin-positive and FMRpolyG-positive inclusions accompanied with impaired motor performance (50). These data suggest a disease-causing role for astroglia in FXTAS. Although all these data presented suggest a disease-causing role for inclusions in neurons and astrocytes, the presence of inclusions might not be related or even protective, as has already been described in patients with hereditary ataxia and polyglutamine diseases (51,52). To date, the role of inclusions in both neurons and astrocytes in the pathogenesis of FXTAS is not clear and needs further research.

The use of small molecules that shield the CGG repeat RNA [reviewed in (43)] has great potential to ameliorate FXTAS. The advantage of therapeutic interventions targeting CGG RNA is that the RNA folds into diverse structures with repeating motifs allowing small chemical compounds to bind these repeating motifs in the RNA repeating transcripts (53). It has been shown that RNA containing an expanded CGG repeat forms hairpin structures with periodically repeating internal GG loops. Several RNA-binding small molecule compounds targeting the internal GG loop of the expanded CGG repeat were developed (42,54–56). One potential liability of small chemical compounds, despite their improved affinities, selectivity and potency, is their high molecular weights, which could decrease cellular and tissue permeability. To overcome this problem, favorable properties of monomeric ligands can be incorporated in the compound to enhance its permeability. Studies using transfected COS7 cells that transiently overexpressed RNA containing an expanded CGG repeat showed that compound *1a* can improve FXTAS-associated pre-mRNA splicing defects and reduce the size and number of nuclear RNA foci. Furthermore, the binding of compound *1a* does not affect the translation of the downstream open reading frame (ORF) (42,57,58). The advantage of this approach is that it prevents RBPs from binding to the hairpin structure and additionally the small molecules will block RAN translation, without having an effect on the translation of *FMR1* mRNA. In the inducible neuronal cultures, the number of intranuclear inclusions is significantly reduced by adding compound *1a* to the culture medium. This suggests that the use of compound *1a* is a promising intervention strategy and it is crucial to test these compounds *in vivo*. Both the ubiquitous expressing and the brain-specific inducible mouse models are excellent models, using survival, liver pathology, neuropathology and animal behavior as the outcome measures. A similar approach has been used for C9FTD/ALS. Small molecule compounds targeting RNA containing the expanded GGGGCC repeat were designed and were found to significantly inhibit RAN translation and foci formation in cultured cells expressing mutant RNA in neurons transdifferentiated from fibroblasts of repeat expansion carriers (56). Given the structural similarity between CGG repeat and GGGGCC repeat, it was expected that compound *1a* might bind the GGGGCC repeat sequence in C9ALS/FTD (43). Recognition and binding of GG motifs by compound *1a* in CG-rich sequences could form a liability for further development of compound *1a* since the effect on CG-rich coding regions is not known. The short CGG repeats in the other genes are less likely to be affected by *1a*. Compound *1a* can bind to the long CGG repeats of FMR1 in FXTAS selectively owing to the greater structural stability and the larger abundance of the 1×1 GG internal loops in the long CGG repeats (56). The fact that *1a* is not restricted to FXTAS only suggests it could be further developed as a multi-disease drug, making it more attractive for big pharmaceutical companies to invest in the future development and improvement of compound *1a*.

Next, we exposed these ubiquitous inducible mice to compound *1a*. Similar to the *in vitro* model, the inducible mouse model shows expression of GFP and CGG_{exp} mRNA after induction with dox. Surprisingly, these mice did not suffer from liver toxicity as was published before by our laboratory in 2014 (40). First, we speculated that the age of the mice at experimental onset might explain the absence of the liver toxicity, but after inducing expression with dox in younger mice, we did not see any signs for liver toxicity. Current hypothesis is that the change in phenotype is owing to the background the mice were bred in. Initially, these mice were bred in the C57BL/6 background, but overtime, we maintained these mice by crossing them with a mouse line having a C57BL/6JRj background. It is known from literature that different mouse strains respond differently to treatments (59). Even though we do not understand in which way the background could have influenced the phenotype and therefore loss of initial functional read-out, we still could show that these mice express the transgene with qRT-PCR, western blot and dot blot. Since these mice lived longer, we hypothesized next that that these mice should be able to develop inclusions in the liver. Indeed, when we sacrificed the mice and examined for the presence of inclusions, we could already detect FMRpolyG-positive inclusions throughout the entire liver within 5 days after dox induction. Using double staining for ubiquitin and Rad23b, we also found both proteins being present in these FMRpolyG-positive inclusions. In addition, we were also able to detect both FMRpolyG and Rad23b in the insoluble protein fractions at the

molecular level. Taken together, these mice have developed a protein aggregation liver pathology without dying, allowing us to rapidly test potential therapeutic interventions.

We could show that upon treatment of the mice with compound *1a*, FMRpolyG levels together with Rad23b levels could be reduced. A striking difference in the results between the *in vitro* and *in vivo* models is that we did not see a significant decrease of the FMRpolyG-positive inclusions in this mouse model. We hypothesize that while there may not be a decrease in the number of inclusions, the inclusions could have decreased in size. The significant decrease in the aggregated FMRpolyG protein level we present in this study supports this hypothesis. In addition, it may be that a second IP injection is necessary to halt the formation of inclusions. Nevertheless, further optimization of compound *1a* is warranted. Importantly, we could reduce the protein levels of FMRpolyG in these mice using a single IP injection. In previous studies, the presence of FMRpolyG-positive inclusions showed a clear effect on behavior and locomotor function (35). Unfortunately, we were not able to show the effect of the compound on motor and cognitive functions. To see whether reduction of the FMRpolyG levels can also rescue the motor and cognitive phenotypes associated with FXTAS, a brain-specific inducible mouse model can be treated with compound *1a*. Further research involving mouse models with brain-specific CGG_{exp} expression that allow for functional analyses on, that is, the compensatory eye movement—of which we observed a phenotype in earlier studies (36)—could be performed as follow-up studies.

While both *in vitro* and *in vivo* models used in this study involve the same inducible mouse models, there are notable differences between the models, such as the speed at which the models develop FMRpolyG-positive inclusions. Inclusions in the *in vivo* model are formed within 5 days after dox induction, whereas in the primary hippocampal neuronal cultures, this process needs approximately 10 days. It is hard to compare protein inclusion formation in both systems and make conclusive remarks on both models since we are comparing two totally different tissue types. Whole liver metabolism and gene expression patterns in a living organism could have accelerating effects on the protein aggregation process. Neurons are regulating cells with a limited capacity for cell renewal, while the liver has a more robust renewal capability and is highly involved in the metabolic processes. Second, in line with the high metabolic activity in the liver, is the effect of dox on neurons and hepatocytes. Dox is an antibiotic derived from the tetracycline family known for its anti-oxidant and anti-inflammatory effects. Even though this is the case for neurons where dox has a more protective and anti-inflammatory role in the brain, in the liver, it mitigates hepatic injury after 1–2 weeks of administration (60,61). Although these mice were sacrificed before any hepatic injury could be detected macroscopically, at the molecular level, dox could have already had its effects inducing stress in the hepatocytes. It is known for *C9ORF72*-linked ALS/FTD and FXTAS that the ISR stimulates the production of RAN translation proteins like FMRpolyG in FXTAS (32).

In addition to the speed at which the inclusions form, the localization of them also differs between the *in vitro* and *in vivo* models. Ubiquitin-positive intranuclear inclusions in neurons and astrocytes are the neuropathological hallmark of FXTAS. In the primary neuronal cell culture model, we show the presence of characteristic intranuclear inclusions in both neurons (excitatory and inhibitory) and astrocytes, illustrating similarities between this model and the post-mortem brain tissue from FXTAS patients (8). However, the inclusions in the *in vivo* model are generally located in the cytoplasm. The speed at which the inclusions form most likely plays a role. Because in our *in vivo* model the inclusions form within 5 days, we hypothesize that upon sacrificing the mice, the aggregates formed were not able to relocate to the nucleus yet (35).

In this present study, we found that *in vivo* Rad23b co-localizes with FMRpolyG in these inclusions. It is an interesting question to ask whether FMRpolyG recruits, for example, Rad23b to the inclusions or that FMRpolyG is sequestered into these inclusions because it is toxic to the cells and aggregation is a way to prevent cellular toxicity and Rad23b is recruited to assist in the protein degradation of FMRpolyG. Previously, many other molecular chaperones like HSP40 and the 20S catalytic core complex of the proteasome were found to also accumulate in these inclusions in mice (37). It is not entirely clear why Rad23b is present in these inclusions. Accumulation of Rad23b in the inclusions can be an effect of a cellular state or serve a more functional role in the cause of these inclusions. It is known that Rad23b interacts with the 26S proteasome for degradation of ubiquitinated proteins (38). Ubiquitylation is a general protein modification process involved in the degradation of misfolded or toxic proteins via sequential process by the ubiquitin-activating enzyme (E1), a ubiquitin-conjugating enzyme (E2) and a specific ubiquitin ligase (E3). Through a ubiquitin-associated domain (UBA), ubiquitinated proteins are recognized and sent to the 26S proteasome for degradation. Although Rad23b has two of these UBA domains, it is protected by an intrinsic stabilization signal (62), making it an ideal candidate to serve for the shuttling of misfolded proteins to be degraded by the 26S proteasome (63,64) and possibly explaining the presence of Rad23b in these inclusions. Another possible hypothesis as why Rad23b co-localizes with FMRpolyG and ubiquitin in these inclusions is because Rad23b has two UBA domains that are capable of binding ubiquitinated proteins that are present in these inclusions. In this *in vivo* inducible mouse model, inclusions were predominantly present in the cytoplasm. Although we do not know the origin or the function of Rad23b in these cytoplasmic inclusions, it might be that Rad23b is also a prelude in the formation of intranuclear inclusions. Overexpression of Rad23b in living cells is known to inhibit 26S proteasome degradation potential (65,66). It is also known that RAN translation of the CGG_{exp} in FXTAS causes impairment in the UPS (34). Despite the fact that no correlation between Rad23b protein levels and proteasome activity *in vivo* has been made in the present study, this may suggest that the UPS is impaired. Impairment in protein degradation by the UPS is directly or indirectly involved in many neurodegenerative disorders, but whether it is a cause or consequence needs further research (67).

Interesting to note is that while *in vivo* treatment with compound *1a* resulted in less Rad23b in the inclusions, there was no significant effect on the number of FMRpolyG-positive inclusions. Although there are several hypotheses about why Rad23b is present in the inclusions, it remains fascinating why compound *1a* affects Rad23b presence in the inclusions but not the FMRpolyG protein. Although the definitive reason remains unclear based on what is aforementioned, we like to hypothesize that upon treatment with compound *1a*, RAN translation is inhibited. This inhibition results in less production of FMRpolyG and potentially stimulates the UPS. Stimulation of the UPS could result in the need for Rad23b to shuttle misfolded and toxic ubiquitinated proteins to the 26S proteasome for degradation, resulting in less Rad23b capture in inclusions. This supports our initial hypothesis that FMRpolyG-positive inclusions may

have decreased in size and not in number and also explain the decreased levels of FMRpolyG.

Supplementary Material

Supplementary Material is available at *HMG* online.

Acknowledgements

The authors wish to acknowledge the contribution of Mirjam Schoof to this work during her internship and thank Nicolas Charlet-Berguerand for the nCGG-GFP plasmids and the FMRpolyG mouse monoclonal antibodies. This work was funded by the Dutch Brain Foundation (project number F2012(1)-101), including project 1-R35-NS116846-01 from the US National Institutes of Health (to M.D.D.).

Conflict of Interest statement. The authors declare that they have no conflicts of interest.

Funding

This work was funded by project F2012(1)-101 from the Dutch Brain Foundation and project 1-R35-NS116846-01 from the US National Institutes of Health (to M.D.D.)

References

1. Hagerman, R.J., Leehey, M., Heinrichs, W., Tassone, F., Wilson, R., Hills, J., Grigsby, J., Gage, B. and Hagerman, P.J. (2001) Intention tremor, parkinsonism, and generalized brain atrophy in male carriers of fragile X. *Neurology*, **57**, 127–130.
2. Leehey, M.A. (2009) Fragile X-associated tremor/ataxia syndrome: clinical phenotype, diagnosis, and treatment. *J. Invest. Med.*, **57**, 830–836.
3. Grigsby, J., Brega, A.G., Seritan, A.L. and Bourgeois, J.A. (2010) FXTAS: neuropsychological/neuropsychiatric phenotypes. In Tassone, F. and Berry-Kravis, E.M. (eds), *The Fragile X-Associated Tremor Ataxia Syndrome (FXTAS)*. Springer, New York, NY, pp. 31–53.
4. Jacquemont, S., Hagerman, R.J., Leehey, M., Grigsby, J., Zhang, L., Brunberg, J.A., Greco, C., Des Portes, V., Jardini, T., Levine, R. *et al.* (2003) Fragile X premutation tremor/ataxia syndrome: molecular, clinical, and neuroimaging correlates. *Am. J. Hum. Genet.*, **72**, 869–878.
5. Hall, D.A., Birch, R.C., Anheim, M., Jønch, A.E., Pintado, E., O'Keefe, J., Trollor, J.N., Stebbins, G.T., Hagerman, R.J., Fahn, S., Berry-Kravis, E. and Leehey, M.A. (2014) Emerging topics in FXTAS. *J. Neurodev. Disord.*, **6**, 31.
6. Brunberg, J.A., Jacquemont, S., Hagerman, R.J., Berry-Kravis, E.M., Grigsby, J., Leehey, M.A., Tassone, F., Brown, W.T., Greco, C.M. and Hagerman, P.J. (2002) Fragile X premutation carriers: characteristic MR imaging findings of adult male patients with progressive cerebellar and cognitive dysfunction. *AJNR Am. J. Neuroradiol.*, **23**, 1757–1766.
7. Greco, C.M., Berman, R.F., Martin, R.M., Tassone, F., Schwartz, P.H., Chang, A., Trapp, B.D., Iwahashi, C., Brunberg, J., Grigsby, J. *et al.* (2006) Neuropathology of fragile X-associated tremor/ataxia syndrome (FXTAS). *Brain*, **129**, 243–255.
8. Greco, C.M., Hagerman, R.J., Tassone, F., Chudley, A.E., Del Bigio, M.R., Jacquemont, S., Leehey, M. and Hagerman, P.J. (2002) Neuronal intranuclear inclusions in a new cerebellar tremor/ataxia syndrome among fragile X carriers. *Brain*, **125**, 1760–1771.
9. Hunsaker, M.R., Greco, C.M., Spath, M.A., Smits, A.P.T., Navarro, C.S., Tassone, F., Kros, J.M., Severijnen, L.A., Berry-Kravis, E.M., Berman, R.F. *et al.* (2011) Widespread non-central nervous system organ pathology in fragile X premutation carriers with fragile X-associated tremor/ataxia syndrome and CGG knock-in mice. *Acta Neuropathol.*, **122**, 467–479.
10. Buijsen, R.A., Sellier, C., Severijnen, L.A.W.F.M., Oulad-Abdelghani, M., Verhagen, R.F.M., Berman, R.F., Charlet-Berguerand, N., Willemsen, R. and Hukema, R.K. (2014) FMRpolyG-positive inclusions in CNS and non-CNS organs of a fragile X premutation carrier with fragile X-associated tremor/ataxia syndrome. *Acta Neuropathol. Commun.*, **2**, 162.
11. Greco, C.M., Soontrapornchai, K., Wirojanan, J., Gould, J.E., Hagerman, P.J. and Hagerman, R.J. (2007) Testicular and pituitary inclusion formation in fragile X associated tremor/ataxia syndrome. *J. Urol.*, **177**, 1434–1437.
12. Gokden, M., Al-Hinti, J.T. and Harik, S.I. (2009) Peripheral nervous system pathology in fragile X tremor/ataxia syndrome (FXTAS). *Neuropathology*, **29**, 280–284.
13. Louis, E., Moskowitz, C., Friez, M., Amaya, M. and Vonsattel, J.P.G. (2006) Parkinsonism, dysautonomia, and intranuclear inclusions in a fragile X carrier: a clinical-pathological study. *Mov. Disord.*, **21**, 420–425.
14. Tassone, F., Hagerman, R.J., Garcia-Arocena, D., Khandjian, E.W., Greco, C.M. and Hagerman, P.J. (2004) Intranuclear inclusions in neural cells with premutation alleles in fragile X associated tremor/ataxia syndrome. *J. Med. Genet.*, **41**, e43.
15. Buijsen, R.A., Visser, J.A., Kramer, P., Severijnen, E.A.W.F.M., Gearing, M., Charlet-Berguerand, N., Sherman, S.L., Berman, R.F., Willemsen, R. and Hukema, R.K. (2016) Presence of inclusions positive for polyglycine containing protein, FMRpolyG, indicates that repeat-associated non-AUG translation plays a role in fragile X-associated primary ovarian insufficiency. *Hum. Reprod.*, **31**, 158–168.
16. Boivin, M., Willemsen, R., Hukema, R.K. and Sellier, C. (2018) Potential pathogenic mechanisms underlying fragile X tremor ataxia syndrome: RAN translation and/or RNA gain-of-function? *Eur. J. Med. Genet.*, **61**, 674–679.
17. Yu, S., Pritchard, M., Kremer, E., Lynch, M., Nancarrow, J., Baker, E., Holman, K., Mulley, J., Warren, S. and Schlessinger, D. (1991) Fragile X genotype characterized by an unstable region of DNA. *Science*, **252**, 1179–1181.
18. Peprah, E., He, W., Allen, E., Oliver, T., Boyne, A. and Sherman, S.L. (2010) Examination of FMR1 transcript and protein levels among 74 premutation carriers. *J. Hum. Genet.*, **55**, 66–68.
19. Kenneson, A., Zhang, F., Hagedorn, C.H. and Warren, S.T. (2001) Reduced FMRP and increased FMR1 transcription is proportionally associated with CGG repeat number in intermediate-length and premutation carriers. *Hum. Mol. Genet.*, **10**, 1449–1454.
20. Tassone, F., Hagerman, R.J., Taylor, A.K., Gane, L.W., Godfrey, T.E. and Hagerman, P.J. (2000) Elevated levels of FMR1 mRNA in carrier males: a new mechanism of involvement in the fragile-X syndrome. *Am. J. Hum. Genet.*, **66**, 6–15.
21. Jacquemont, S., Hagerman, R.J., Leehey, M.A., Hall, D.A., Levine, R.A., Brunberg, J.A., Zhang, L., Jardini, T., Gane, L.W., Harris, S.W. *et al.* (2004) Penetrance of the fragile X-associated tremor/ataxia syndrome in a premutation carrier population. *JAMA*, **291**, 460–469.
22. Rodriguez-Revenga, L., Madrigal, I., Pagonabarraga, J., Xunclà, M., Badenas, C., Kulisevsky, J., Gomez, B. and Milà, M. (2009) Penetrance of FMR1 premutation associated pathologies in fragile X syndrome families. *Eur. J. Hum. Genet.*, **17**, 1359–1362.

23. Sellier, C., Usdin, K., Pastori, C., Peschansky, V.J., Tassone, F. and Charlet-Berguerand, N. (2014) The multiple molecular facets of fragile X-associated tremor/ataxia syndrome. *J. Neurodev. Disord.*, **6**, 23.
24. Sellier, C., Rau, F., Liu, Y., Tassone, F., Hukema, R.K., Gattoni, R., Schneider, A., Richard, S., Willemsen, R., Elliott, D.J., Hagerman, P.J. and Charlet-Berguerand, N. (2010) Sam68 sequestration and partial loss of function are associated with splicing alterations in FXTAS patients. *EMBO J.*, **29**, 1248–1261.
25. Sellier, C., Freyermuth, F., Tabet, R., Tran, T., He, F., Ruffenach, F., Alunni, V., Moine, H., Thibault, C., Page, A. *et al.* (2013) Sequestration of DROSHA and DGCR8 by expanded CGG RNA repeats alters microRNA processing in fragile X-associated tremor/ataxia syndrome. *Cell Rep.*, **3**, 869–880.
26. Jin, P., Duan, R., Qurashi, A., Qin, Y., Tian, D., Rosser, T.C., Liu, H., Feng, Y. and Warren, S.T. (2007) Pur alpha binds to rCGG repeats and modulates repeat-mediated neurodegeneration in a *Drosophila* model of fragile X tremor/ataxia syndrome. *Neuron*, **55**, 556–564.
27. Sofola, O.A., Jin, P., Qin, Y., Duan, R., Liu, H., de Haro, M., Nelson, D.L. and Botas, J. (2007) RNA-binding proteins hnRNP A2/B1 and CUGBP1 suppress fragile X CGG premutation repeat-induced neurodegeneration in a *Drosophila* model of FXTAS. *Neuron*, **55**, 565–571.
28. Zu, T., Gibbens, B., Doty, N.S., Gomes-Pereira, M., Huguet, A., Stone, M.D., Margolis, J., Peterson, M., Markowski, T.W., Ingram, M.A.C. *et al.* (2011) Non-ATG-initiated translation directed by microsatellite expansions. *Proc. Natl. Acad. Sci. U. S. A.*, **108**, 260–265.
29. Todd, P.K., Oh, S.Y., Krans, A., He, F., Sellier, C., Frazer, M., Renoux, A.J., Chen, K.C., Scaglione, K.M., Basrur, V. *et al.* (2013) CGG repeat-associated translation mediates neurodegeneration in fragile X tremor ataxia syndrome. *Neuron*, **78**, 440–455.
30. Nguyen, L., Cleary, J.D. and Ranum, L.P.W. (2019) Repeat-associated non-ATG translation: molecular mechanisms and contribution to neurological disease. *Annu. Rev. Neurosci.*, **42**, 227–247.
31. Kearse, M.G., Green, K.M., Krans, A., Rodriguez, C.M., Linsalata, A.E., Goldstrohm, A.C. and Todd, P.K. (2016) CGG repeat-associated non-AUG translation utilizes a cap-dependent scanning mechanism of initiation to produce toxic proteins. *Mol. Cell*, **62**, 314–322.
32. Green, K.M., Glineburg, M.R., Kearse, M.G., Flores, B.N., Linsalata, A.E., Fedak, S.J., Goldstrohm, A.C., Barmada, S.J. and Todd, P.K. (2017) RAN translation at C9orf72-associated repeat expansions is selectively enhanced by the integrated stress response. *Nat. Commun.*, **8**, 2005.
33. Haify, S.N., Botta-Orfila, T., Hukema, R.K. and Tartaglia, G.G. (2020) In silico, in vitro, and in vivo approaches to identify molecular players in fragile X tremor and ataxia syndrome. *Front. Mol. Biosci.*, **7**, 31.
34. Oh, S.Y., He, F., Krans, A., Frazer, M., Taylor, J.P., Paulson, H.L. and Todd, P.K. (2015) RAN translation at CGG repeats induces ubiquitin proteasome system impairment in models of fragile X-associated tremor ataxia syndrome. *Hum. Mol. Genet.*, **24**, 4317–4326.
35. Sellier, C., Buijsen, R.A.M., He, F., Natla, S., Jung, L., Tropel, P., Gaucherot, A., Jacobs, H., Meziane, H., Vincent, A. *et al.* (2017) Translation of expanded CGG repeats into FMRpolyG is pathogenic and may contribute to fragile X tremor ataxia syndrome. *Neuron*, **93**, 331–347.
36. Hukema, R.K., Buijsen, R.A.M., Schonewille, M., Raske, C., Severijnen, L.A.W.F.M., Nieuwenhuizen-Bakker, I., Verhagen, R.F.M., van Dessel, L., Maas, A., Charlet-Berguerand, N. *et al.* (2015) Reversibility of neuropathology and motor deficits in an inducible mouse model for FXTAS. *Hum. Mol. Genet.*, **24**, 4948–4957.
37. Willemsen, R., Hoogeveen-Westerveld, M., Reis, S., Holstege, J., Severijnen, L.A., Nieuwenhuizen, I.M., Schrier, M., van Unen, L., Tassone, F., Hoogeveen, A.T. *et al.* (2003) The FMR1 CGG repeat mouse displays ubiquitin-positive intranuclear neuronal inclusions; implications for the cerebellar tremor/ataxia syndrome. *Hum. Mol. Genet.*, **12**, 949–959.
38. Bergink, S., Severijnen, L.A., Wijgers, N., Sugasawa, K., Yousaf, H., Kros, J.M., van Swieten, J., Oostra, B.A., Hoeijmakers, J.H., Vermeulen, W. and Willemsen, R. (2006) The DNA repair-ubiquitin-associated HR23 proteins are constituents of neuronal inclusions in specific neurodegenerative disorders without hampering DNA repair. *Neurobiol. Dis.*, **23**, 708–716.
39. Hashem, V., Galloway, J.N., Mori, M., Willemsen, R., Oostra, B.A., Paylor, R. and Nelson, D.L. (2009) Ectopic expression of CGG containing mRNA is neurotoxic in mammals. *Hum. Mol. Genet.*, **18**, 2443–2451.
40. Hukema, R.K., Buijsen, R.A., Raske, C., Severijnen, L.A., Nieuwenhuizen-Bakker, I., Minneboo, M., Maas, A., de Crom, R., Kros, J.M., Hagerman, P.J., Berman, R.F. and Willemsen, R. (2014) Induced expression of expanded CGG RNA causes mitochondrial dysfunction in vivo. *Cell Cycle*, **13**, 2600–2608.
41. Gunal, D.I., Afşar, N., Bekiroglu, N. and Aktan, S. (2000) New alternative agents in essential tremor therapy: double-blind placebo-controlled study of alprazolam and acetazolamide. *Neurol. Sci.*, **21**, 315–317.
42. Disney, M.D., Liu, B., Yang, W.Y., Sellier, C., Tran, T., Charlet-Berguerand, N. and Childs-Disney, J.L. (2012) A small molecule that targets r(CGG)(exp) and improves defects in fragile X-associated tremor ataxia syndrome. *ACS Chem. Biol.*, **7**, 1711–1718.
43. Childs-Disney, J.L. and Disney, M.D. (2016) Approaches to validate and manipulate RNA targets with small molecules in cells. *Annu. Rev. Pharmacol. Toxicol.*, **56**, 123–140.
44. Yang, W.Y., He, F., Strack, R.L., Oh, S.Y., Frazer, M., Jaffrey, S.R., Todd, P.K. and Disney, M.D. (2016) Small molecule recognition and tools to study modulation of r(CGG)(exp) in fragile X-associated tremor ataxia syndrome. *ACS Chem. Biol.*, **11**, 2456–2465.
45. Seibenhener, M.L. and Wooten, M.W. (2012) Isolation and culture of hippocampal neurons from prenatal mice. *J. Vis. Exp.*, **65**, 3634. doi: 10.3791/3634.
46. Zakeri, B. and Wright, G.D. (2008) Chemical biology of tetracycline antibiotics. *Biochem. Cell Biol.*, **86**, 124–136.
47. Motulsky, H.J. *Graphpad Statistics Guide*. California (USA), Scott Adams. Cited 2020; Available from: http://www.graphpad.com/guides/prism/7/statistics/index.htm.
48. Iwahashi, C.K., Yasui, D.H., An, H.J., Greco, C.M., Tassone, F., Nannen, K., Babineau, B., Lebrilla, C.B., Hagerman, R.J. and Hagerman, P.J. (2006) Protein composition of the intranuclear inclusions of FXTAS. *Brain*, **129**, 256–271.
49. van Dam, D., Errijgers, V., Kooy, R.F., Willemsen, R., Mientjes, E., Oostra, B.A. and de Deyn, P.P. (2005) Cognitive decline, neuromotor and behavioural disturbances in a mouse model for fragile-X-associated tremor/ataxia syndrome (FXTAS). *Behav. Brain Res.*, **162**, 233–239.

50. Wenzel, H.J., Hunsaker, M.R., Greco, C.M., Willemsen, R. and Berman, R.F. (2010) Ubiquitin-positive intranuclear inclusions in neuronal and glial cells in a mouse model of the fragile X premutation. *Brain Res.*, **1318**, 155–166.
51. Zoghbi, H.Y. and Botas, J. (2002) Mouse and fly models of neurodegeneration. *Trends Genet.*, **18**, 463–471.
52. Saudou, F., Finkbeiner, S., Devys, D. and Greenberg, M.E. (1998) Huntingtin acts in the nucleus to induce apoptosis but death does not correlate with the formation of intranuclear inclusions. *Cell*, **95**, 55–66.
53. Swayze, E.E. and Bhat, B. (2007) The medicinal chemistry of oligonucleotides. In Crooke, S.T. (ed), (ed)*Antisense Drug Technology: Principles, Strategies, and Applications*, 2nd edn. Taylor & Francis, United Kingdom, pp. 143–182.
54. Parkesh, R., Childs-Disney, J.L., Nakamori, M., Kumar, A., Wang, E., Wang, T., Hoskins, J., Tran, T., Housman, D., Thornton, C.A. and Disney, M.D. (2012) Design of a bioactive small molecule that targets the myotonic dystrophy type 1 RNA via an RNA motif-ligand database and chemical similarity searching. *J. Am. Chem. Soc.*, **134**, 4731–4742.
55. Lee, M.M., Pushechnikov, A. and Disney, M.D. (2009) Rational and modular design of potent ligands targeting the RNA that causes myotonic dystrophy 2. *ACS Chem. Biol.*, **4**, 345–355.
56. Su, Z., Zhang, Y., Gendron, T.F., Bauer, P.O., Chew, J., Yang, W.Y., Fostvedt, E., Jansen-West, K., Belzil, V.V., Desaro, P. *et al.* (2014) Discovery of a biomarker and lead small molecules to target r(GGGGCC)-associated defects in c9FTD/ALS. *Neuron*, **83**, 1043–1050.
57. Tran, T., Childs-Disney, J.L., Liu, B., Guan, L., Rzuczek, S. and Disney, M.D. (2014) Targeting the r(CGG) repeats that cause FXTAS with modularly assembled small molecules and oligonucleotides. *ACS Chem. Biol.*, **9**, 904–912.
58. Yang, W.Y., Wilson, H.D., Velagapudi, S.P. and Disney, M.D. (2015) Inhibition of non-ATG translational events in cells via covalent small molecules targeting RNA. *J. Am. Chem. Soc.*, **137**, 5336–5345.
59. Yoshiki, A. and Moriwaki, K. (2006) Mouse phenome research: implications of genetic background. *ILAR J.*, **47**, 94–102.
60. Meli, D.N., Coimbra, R.S., Erhart, D.G., Loquet, G., Bellac, C.L., Täuber, M.G., Neumann, U. and Leib, S.L. (2006) Doxycycline reduces mortality and injury to the brain and cochlea in experimental pneumococcal meningitis. *Infect. Immun.*, **74**, 3890–3896.
61. (2012) LiverTox: clinical and research information on drug-induced liver injury. https://pubmed.ncbi.nlm.nih.gov/31643176/.
62. Heessen, S., Masucci, M.G. and Dantuma, N.P. (2005) The UBA2 domain functions as an intrinsic stabilization signal that protects Rad23 from proteasomal degradation. *Mol. Cell*, **18**, 225–235.
63. Varadan, R., Assfalg, M., Raasi, S., Pickart, C. and Fushman, D. (2005) Structural determinants for selective recognition of a Lys48-linked polyubiquitin chain by a UBA domain. *Mol. Cell*, **18**, 687–698.
64. Verma, R., Oania, R., Graumann, J. and Deshaies, R.J. (2004) Multiubiquitin chain receptors define a layer of substrate selectivity in the ubiquitin-proteasome system. *Cell*, **118**, 99–110.
65. Ortolan, T.G., Tongaonkar, P., Lambertson, D., Chen, L., Schauber, C. and Madura, K. (2000) The DNA repair protein rad23 is a negative regulator of multi-ubiquitin chain assembly. *Nat. Cell Biol.*, **2**, 601–608.
66. Raasi, S. and Pickart, C.M. (2003) Rad23 ubiquitin-associated domains (UBA) inhibit 26 S proteasome-catalyzed proteolysis by sequestering lysine 48-linked polyubiquitin chains. *J. Biol. Chem.*, **278**, 8951–8959.
67. Glickman, M.H. and Ciechanover, A. (2002) The ubiquitin-proteasome proteolytic pathway: destruction for the sake of construction. *Physiol. Rev.*, **82**, 373–428.